



LJMU Research Online

Cherian, T, Ragavendran, C, Remesh, RKV, Jacob, J, Jamal, W, Kamaraj, C and Nakouti, I

Bio-functionalization, stabilization and potential functionalities of hyaluronate macromolecules capped copper oxide nanoparticles

<http://researchonline.ljmu.ac.uk/id/eprint/21683/>

Article

Citation (please note it is advisable to refer to the publisher's version if you intend to cite from this work)

Cherian, T, Ragavendran, C, Remesh, RKV, Jacob, J, Jamal, W, Kamaraj, C and Nakouti, I (2023) Bio-functionalization, stabilization and potential functionalities of hyaluronate macromolecules capped copper oxide nanoparticles. Journal of Environmental Chemical Engineering. 11 (6). ISSN

LJMU has developed [LJMU Research Online](#) for users to access the research output of the University more effectively. Copyright © and Moral Rights for the papers on this site are retained by the individual authors and/or other copyright owners. Users may download and/or print one copy of any article(s) in LJMU Research Online to facilitate their private study or for non-commercial research. You may not engage in further distribution of the material or use it for any profit-making activities or any commercial gain.

The version presented here may differ from the published version or from the version of the record. Please see the repository URL above for details on accessing the published version and note that access may require a subscription.

For more information please contact researchonline@ljmu.ac.uk

<http://researchonline.ljmu.ac.uk/>

1 **Bio-functionalization, stabilization and potential functionalities of hyaluronate**
2 **macromolecules capped copper oxide nanoparticles**

3 **Tijo Cherian^{1*}, Chinnasamy Ragavendran^{2**}, Roshan K V Remesh³, Wajih Jamal⁴,**
4 **Jenny Jacob¹, Chinnaperumal Kamaraj⁵, Ismini Nakouti^{6***}**

5 ¹School of Biosciences, Mar Athanasios College for Advanced Studies Tiruvalla
6 (MACFAST), Tiruvalla, Kerala-689101, India

7 ²Department of Conservative Dentistry and Endodontics, Saveetha Dental College and
8 Hospitals, Saveetha Institute of Medical and Technical Sciences (SIMATS), Chennai,
9 India

10 ³Department of Biotechnology, Sree Narayana Arts and Science College, Kumarakom,
11 Kottayam, Kerala- 686563, India

12 ⁴Department of Zoology, Aligarh Muslim University, Aligarh, Uttar Pradesh, India
13 202002

14 ⁵Interdisciplinary Institute of Indian System of Medicine (IIISM), SRM Institute Science
15 and Technology, Kattankulathur-603 203, Tamil Nadu, India

16 ⁶Centre for Natural Products Discovery (CNPD), School of Pharmacy and Biomolecular
17 Sciences, Liverpool John Moores University, Liverpool L3 3AF, UKE. mail:
18 I.Nakouti@ljmu.ac.uk

19 ***Corresponding authors:**

20 1. **Tijo Cherian:** School of Biosciences, Mar Athanasios College for Advanced Studies
21 Tiruvalla (MACFAST), Tiruvalla, Kerala-689101, India. E.mail:
22 tvarghese891@gmail.com.

23 2. **Chinnasamy Ragavendran:** Department of Conservative Dentistry and Endodontics,
24 Saveetha Dental College and Hospitals, Saveetha Institute of Medical and Technical
25 Sciences (SIMATS), Chennai, India. E. mail: ragavan889@gmail.com.

26 3. **Ismiini Nakouti:** Centre for Natural Products Discovery (CNPD), School of Pharmacy
27 and Biomolecular Sciences, Liverpool John Moores University, Liverpool L3 3AF, UK
28 E.mail: I.Nakouti@ljmu.ac.uk

29

30 **Abstract**

31 The optical-electrical properties of CuO-NPs (copper oxide nanoparticles) are
32 being expanded widely for high-technological uses. In accordance with the idea of an
33 eco-friendly synthesis process, CuO-NPs were synthesized utilizing a safer method;
34 stabilized by biopolymer sodium hyaluronate (SH) rather than a hazardous substance.
35 Using one variable at one time method with constant reaction variables, the synthesis
36 parameters were optimized and the characteristics of CuO-NPs were controlled. The
37 resulting particles exhibited restricted distribution, were typically round or oval in form
38 and particle size of 17 ± 1.3 nm (by TEM and SEM), strongly crystalline (by XRD) and
39 were noticeably stable. The experimental analysis of FT-IR documented that the redox
40 reaction between biopolymers and metal cations; coupled by capping effect of thin layer
41 of SH-macromolecules, are primarily responsible for the formation and stabilization of
42 CuO-NPs. Also, CuO-NPs exhibited strong bactericidal (ZOI 22-27 nm; antibiofilm
43 potential 71-85%), anti-diabetic (70-72%), DNA cleavage and antioxidant activity (70-
44 85%). Additionally, SH-stabilized CuO-NPs demonstrated catalytic activity for the
45 reduction of catalytic dyes, degrading at a rate of over 91-93% in about 10 to 20 min.
46 The current synthetic technique may be applied consecutively to synthesize catalytically
47 active CuO-NPs which exhibited remarkable *in-vitro* biological and biomedical
48 capabilities, possessing the potential to be exploited as a broad-based agent in a variety
49 of biomedical and industrial processes, including the treatment of wastewater.

50 **Keywords:** Sodium hyaluronate, CuO-NPs, Wastewater treatment, Dye degradation,
51 Antioxidant, Antibacterial activity

52

53

54 **1. Introduction**

55 With numerous applications spanning from engineering to health,
56 nanotechnology has emerged as one of the most inventive domains of science and
57 technology [1]. These nanoscale materials have been fabricated using a variety of
58 techniques, including physical, chemical, and environmentally friendly ways; however,
59 these techniques have many shortcomings. Due to their biocompatibility, safety, low
60 toxicity, and cost-effectiveness, green approaches have replaced previous conventional
61 manufacturing techniques for nanoparticles (NPs) over the past few decades [2,3]. The
62 term "Green" refers to the usage of plant-based materials, and "Green nanotechnology"
63 is a subfield of green technology that draws on the ideas of green engineering and green
64 chemistry [4]. Through the use of fewer resources and renewable variables, it decreases
65 the consumption of fuel and energy. Furthermore, by conserving water, energy, and
66 raw materials, as well as by lowering emissions of greenhouse gases and toxic waste;
67 nano-technological goods, procedures, and uses are anticipated to greatly contribute
68 to climatic and environmental protection [1]. The key benefits of green nanotechnology
69 include increased energy efficiency, reduction in waste and emissions of greenhouse
70 gases, and reduced utilization of non-renewable resources. Now-a-days, eco-
71 benevolent nanotechnology syntheses entail the production of NPs without the use of
72 toxic materials that result in harmful byproducts. In other words, the sustainable
73 technique is a way to synthesize nanoparticles that are eco-friendly and doesn't harm
74 biodiversity or human health. It is entirely plausible that current conventional
75 manufacturing processes can produce NPs with exact morphology and size in vast
76 quantities. These techniques, however, use time-consuming, difficult, toxic, and
77 expensive manufacturing methods [5]. Green approaches have many advantages over

78 traditional physical and chemical methods, including quick, simple manufacturing
79 protocols, ease of use, economy, and less waste product formation [6]. Green
80 engineering and chemistry are the foundations upon which green nanotechnology is
81 built, rather than ascend de novo. Green nanotechnology applications could include the
82 utilization of nanomaterials in clean production procedures that synthesize
83 nanoparticles using solar radiations or recycling industrial waste products into
84 nanomaterials, besides the development of fuel cells, biofuels, and solar cells [1,4].
85 There is some "truly" green nanotechnology, such as the full growth of nanoparticles in
86 plants, but these efforts are unlikely to achieve the scale needed for the manufacture of
87 nanomaterials on industrial scale. Green nanotechnology requires a thorough process
88 evaluation in order to get definitive outcomes, much like other industrially produced
89 goods.

90 One of the most practical possibilities among the green approaches available is
91 the biological reduction of metallic cations to neutral ions; subsequent stabilization
92 utilizing a natural template. In order to keep the particle exceedingly stable and
93 catalytically effective by preventing aggregation, this technique normally requires the
94 addition of a template or supporting agent [7]. The employed biotemplate can be
95 derived from biological polymers, dendrimers, organic ligands, plants, different
96 polysaccharides [8,9]. Plant phytochemicals require a supplementary process in the
97 extraction of required substances pre-application because they contain more active
98 components than chemical approaches do. It is difficult to separate and purify
99 manufactured nanoparticles from plant matter [10,11]. In addition, other
100 environmentally friendly synthesis methods, such the production of nanomaterials with
101 the assistance of microorganisms, are ineffective and expensive because to the need for
102 special tools to handle the microbes. According to this theory, naturally occurring

103 carbohydrates that are readily available, for example glucose, pectin, starch, chitin, agar,
104 maltose, arabinose provide a much better starting point in the synthetic process of metal
105 nanoparticles [12]. Such carbohydrate polymeric substances which have large number
106 of structurally bound hydroxyl and carboxylic groups can reduce the metallic salts
107 while also stabilizing the produced nanoparticles. Many scientific literatures have
108 reported a variety of types of carbohydrates, including alginate, chitosan [13-15],
109 carrageen [16,17], cellulose [18], and konjac [19,20], in the fabrication of very stable
110 metal nanoparticles with no aggregation, homogeneous shape and size, high
111 crystallinity, and good catalytic reduction efficiency [21]. The goal of the present work is
112 to develop catalytically efficient CuO-NPs based on sustainable chemistry principles by
113 investigating how SH functions as a stabilizer and reductant of metal precursors.

114 Sodium hyaluronate (SH), classified as glycosaminoglycan, is a long-chain dense
115 biopolymer made of disaccharide monomers of Na-glucuronate-N-acetylglucosamine
116 [22]. It has a variety of uses, including medications (intra-articular injection, creams,
117 etc.), food manufacturing (dietary management for maintaining the amount of
118 carbohydrates), plastic surgery of the skin, and cosmetics for wound healing [21]. In
119 addition to these applications, given that they include a significant amount of hydroxyl
120 and carboxyl groups, it can also be utilized to stabilize metallic particles during the
121 production of nanoparticles. Moreover, SH has been extensively researched for its
122 functions as a template, stabilizer, and reductant for the synthesis of metallic
123 nanoparticles. For instance, SH conjugated metallic nanoparticles have been reported in
124 wide ranging applications like (i) SH-reduced iron oxide nanoparticles for tracking
125 medication and imaging delivery to cancerous cells [23]; (ii) SH-ZnONPs as anti-tumors
126 [24] and wound healing relevance [25]; (iii) SH-AgNPs matrices for antibacterial activity
127 [26]; (iv) chemical reduced SH templated AgNPs in biosensing [27]; (v) AgNPs

128 decorated SH fibers in wound dressing and healing [28]; (vi) cetyl trimethyl
129 ammonium bromide (CTAB)-SH stabilizer in the fabrication of silver nanowires
130 [29];(vii) SH capped silver nanoparticles for in-vivo imaging [30]; (viii) Tween 80
131 coupled SH in the synthesis of nano silver for cellular level targeted drug delivery [31].
132 To the best of the authors' knowledge, there has never been an easy-to-read study
133 explaining wide applicative insights with CuO-NPs that have been reduced and
134 stabilized using a sustainable synthesis procedure. The few relevant works on SH-
135 assisted metal nanoparticles that have been published should be noted; nonetheless,
136 their synthesis processes and end products differ greatly from those of our study. For
137 exemplar, (i) SH-capped nanogold was synthesized by employing the technique of γ -
138 irradiation [32]; (ii) SH assembled gold nanoclusters were fabricated by photodynamic
139 ablation [33]; (iii) glycosaminoglycans stabilized AgNPs were applied as an efficient
140 anti-coagulant and anti-inflammatory agents [34]. Therefore, it is evident that SH-
141 assisted CuO-NPs have not been reported for wide scale applications in various
142 biological fields.

143 Due to their large surface area and small size, metallic nanoparticles have a wide
144 range of uses. Among metal or metal-based nanoparticles, CuO-NPs (copper oxide
145 nanoparticles), a type of metallic nanoparticle, have been applied in a variety of fields,
146 such as catalysis, textile, biomedical, and biosensing [35-38]. Additionally, CuO is more
147 affordable than silver, mixes well with polymers, and has relatively stable physical and
148 chemical characteristics. For the generation of CuO-NPs, a variety of natural sources,
149 such as plants, microorganisms, and fungus, are used [39,40]. Vitamins, carbohydrates,
150 phenolics, and flavonoids are few of the biomolecules and metabolites found in plant
151 extract. These substances have the ability to reduce and stabilize substances as well as
152 convert Cu^{2+} ions into CuO-NPs [41]. Free radical overproduction in the body is a major

153 factor in the development of degenerative conditions like cancer, cataracts,
154 cardiovascular disease, brain dysfunction, and a weaker immune system [42].
155 Antioxidants can, however, neutralize these free radicals before they assault bodily cells
156 and cause disease. Particularly well-known for efficiently scavenging oxygen-
157 containing free radicals are CuO-NPs [43]. Due to their large surface areas and peculiar
158 crystal surface morphologies, metal and metal-based nanoparticles are of great
159 significance. Along with their antioxidant properties, CuO-NPs also have antibacterial
160 properties that are effective against pathogenic bacterial strains [1, 3, 44].

161 Textile manufacturing units are one of the largest sources of wastewater and
162 effluents since they use enormous volumes of synthetic dye compounds, solvent, and
163 auxiliaries during various processing steps [45, 46]. Approximately, 5000 tons of dyes
164 and its auxiliaries are discarded into the aquatic environment each year due to the huge
165 volumes of effluents' unsuitability for reuse. These effluents are extremely poisonous,
166 aesthetically detrimental, mutagenic and carcinogenic in nature [47]. Strong colour,
167 high TDS (total dissolved solids), high chemical oxygen demand (COD), limited
168 biodegradability and changing pH are some of the characteristics of this effluent [21].
169 The textile units frequently modify the dyeing process's colour palette, which results in
170 considerable modifications to the properties of effluents, particularly in terms of COD,
171 pH, colour, and turbidity [48]. Additionally, even if the dye-contaminated effluents
172 undergo small level breakdown, dye molecules are structurally stable creating harmful
173 poisonous chemicals including benzidine, naphthalene, and other aromatic compounds
174 [21]. Many governments enact strong regulations to prevent the use of harmful colours
175 (such azo) and uphold minimum standards for water quality before discharges. Alas,
176 the realistic usage of such dangerous dye compounds has not been eliminated because
177 of their accessibility, cost-compatibility, and remarkable dyeability [1]. As remedial

178 steps, the most popular technique for treating industrial wastewater flocculation or
179 coagulation have been in practice since it efficiently tackles the problems of turbidity,
180 odour, and colour and is straightforward in application [49]. However, there are
181 significant disadvantages to this conventional approach for treating textile wastewater,
182 including high energy and chemical consumption as well as outlay expenditure for the
183 dosage per tank units. Additionally, it creates sludge, which needs additional treatment
184 before disposal because it is regarded as a secondary contaminant [50]. As a result, the
185 treatment of raw textile industry effluents has become urgently in need of an integrated
186 process. As an alternative, advanced technology known as catalytic oxidation has lately
187 been used to decompose poisonous and dangerous organic contaminants [51, 52].
188 Additionally, it is used in the decomposition of lignin in wood pulp and unwanted
189 stains on clothing. Recent years have seen a substantial increase in research into metallic
190 and metallic oxide derived nano catalysts utilized in the catalytic degradation of
191 pollutants in both scientific and industrial worlds [53]. This is a result of their special
192 characteristics such as high catalytic effectiveness, high surface area to volume ratio,
193 efficient active site diffusion, simple scattering of the reactants to the surface of
194 nanoparticles and simple elimination of contaminants from the solution [1].
195 Additionally, recent advances in nano catalysts and nanomaterials were thoroughly
196 investigated, and their potential applications in water purification, wastewater
197 remediation, biosafety, toxicity, and other fields [54, 55]. When compared to other
198 nanomaterials, copper oxide nanoparticles (CuO-NPs) as nano catalysts stand out due
199 to their unique and promising characteristics, such as a simple manufacturing
200 technique, effective catalytic activity, nanoscale dimension, and improved optical
201 behavior [56-58]. Herein, the current study aims to use sodium hyaluronate as a
202 capping/reducing agent in the biosynthesis of CuO-NP and to scrutinize the potential of

203 SH assisted CuO-NPs for myriad biological applications. This is the first investigation
204 on the synthesis of copper oxide nanoparticles using SH. The CuO-NPs were examined
205 for their biological potential utilizing a variety of in-vitro assays, spectroscopic and
206 analytical methods. Additionally, the biosynthesized CuO-NPs were used to investigate
207 the antioxidant and dye degradative efficiency in order to forecast their potential for
208 pharmaceutical use and water treatment practices.

209 **2. Materials and methods**

210 **2.1 Chemicals**

211 Sodium hyaluronate (SH; molecular weight, $M_w = 300000$ g/mol), copper acetate
212 monohydrate ($M_w = 199.65$ g/mol), sodium borohydride (NaBH_4), nutrient broth (NB),
213 Mueller–Hinton agar (MHA) and sodium hydroxide (NaOH) was purchased from
214 Sigma Aldrich. The molecular grade absolute ethanol, model azo dyes [RY145 (reactive
215 yellow 145) and RR195 (reactive red 195)], were purchased from Hi-Media, India. All
216 chemicals used in the study were 97-98% in purity and the respective solutions were
217 prepared using sterile distilled water.

218 **2.2. Synthesis of SH-assisted CuO-NPs**

219 The aqueous solution of SH was prepared by cautiously mixing powdered SH
220 into sterile distilled water under continuous swirling by vortex mixer. (Since, SH is
221 sparingly water soluble, it binds to water molecules instantaneously forming gel).
222 Therefore, the initial mixture was constantly stirred till no visible lumping. Following,
223 the prepared SH solution was mixed with metal solution of copper acetate. Various
224 temperature of temperature-controlled water was applied to the combined solution for
225 a predetermined amount of time. The process parameters were methodically
226 investigated one aspect at a time in order to regulate the final characteristics of

227 synthesized CuO-NPs and optimize the synthesis conditions. The variables were:
228 reaction temperature (30, 40, 50, 60, 70°C), reducing/stabilizing agent concentration
229 (0.05, 0.10, 0.15, 0.20, 0.25%), incubation duration (10, 20, 30, 40, 50 min), and solution
230 pH (4, 6, 8, 10, 12). The final step was to cool and store the synthesized CuO-NPs at
231 room temperature for 24 hours till further characterization. This was done in
232 accordance with the determined optimal conditions, which called for heating a
233 combination of 0.1 mM copper acetate and 0.15% SH for 40 min at 50°C.

234 **2.3. Characterization and measurement**

235 The characterization techniques of ultra-violet visible spectrophotometer, XRD
236 (X-ray diffraction), FT-IR (Fourier transforms infrared spectroscopy), SEM (scanning
237 electron microscopy), high-resolution TEM (transmission electron microscopy), EDX
238 (energy disperse X-ray spectroscopy) were used to characterize CuO-NPs synthesized
239 under ideal conditions. To calculate the efficiency of the catalytic process, the
240 degradation of the azo dye in the presence of CuO-NPs and sodium borohydride was
241 studied. The characterization methods and instrument requirements followed the
242 guidelines mentioned in our earlier report of [1].

243 **2.4 Anti-diabetic potential of CuO-NPs**

244 **2.4.1 α -Amylase inhibition assay**

245 α -amylase inhibition test was determined for analyzing the anti-diabetic
246 potential of CuO-NPs [59]. In brief, 25 μ l of α -amylase enzyme (0.14 U ml⁻¹) +15 μ l
247 phosphate buffer (pH 6.8) were mixed in a sterile 96 well plate. Following, CuO-NPs (10
248 μ l; concentrations 20-100 μ g/ml) and starch solution (40 μ l) were mixed and incubated
249 for 30 minutes at 50°C. Post incubation, iodine reagent (90 μ l; 5 mM potassium iodide, 5
250 mM iodine) and 1M HCl (20 μ l) were added to the resulting mixture. The reaction

251 controls: positive control (acarbose); negative control (solution without test sample) and
252 blank (solution devoid of CuO-NPs and enzyme) were taken in parallel. The optical
253 density of reaction solution was measured at 595 nm and the % enzyme inhibition was
254 evaluated by using following equation (Eq. 1):

$$255 \quad \% \text{ Enzyme inhibition} = OD(s) - \frac{OD(n)}{OD(b)} \times 100 \quad \text{----- (Eq. 1)}$$

256 where OD (n) stands for a negative reference, OD (b) for a blank, and OD (s) for the test
257 sample's absorption value.
258

259 **2.4.2 *In vitro* α -glucosidase inhibition assay**

260 The α -glucosidase inhibition potential of CuO-NPs was ascertained by the
261 protocol of [60] with slight alterations. The reaction mixture: α -glucosidase (7.5 μ l; stock
262 solution (0.5 U/ml) in 20 mmol/l sodium phosphate buffer, pH 6.9) mixed with SH,
263 CuO-NPs (20-100 μ g/ml) and acarbose was kept at 37°C for 15 min. Further, p-
264 nitrophenyl- α -glucopyranoside (PNPG; 100 μ l) was added followed by incubation for 10
265 min at 37°C. Finally, sodium carbonate (Na₂CO₃) (100 μ l; 0.1 M) was mixed to arrest
266 reaction. The absorbance values were read at 405 nm and acarbose was used as
267 reference and control (PNPG + α -glucosidase).

$$268 \quad \% \text{ inhibition} = \frac{\text{control OD} - \text{test OD}}{\text{control OD}} \times 100 \quad \text{----- (Eq. 2)}$$

269 **2.4.3 Non-enzymatic a-glycosylation of hemoglobin (HbA1c)**

270 The biosynthesized CuO-NPs were used in a typical HbA1c inhibition test
271 utilizing the HbA1c technique, with slight modifications [61]. Using 0.01 M phosphate
272 buffer (pH 7.4) as the reaction medium, the arrangement of glucose (2%), haemoglobin
273 (0.06%), and sodium azide (0.02%) were thoroughly mixed. At room temperature,
274 different concentrations of CuO-NPs (20-100 μ g/ml) were mixed with the preceding

275 response mixture. The completed reaction mixture was incubated at room temperature
276 for 72 h under dark environment. The levels of HbA1c inhibition were read at 520 nm
277 and contrasted with those of a common medication like metformin.

278 **2.4.4 Urease inhibition assay**

279 To ascertain urease inhibition activity [62], the reaction mixture (10 μ l CuO-NPs,
280 phosphate buffer (50 μ l, 3 mM, pH 4.5), 100 mM urea, 25 μ l urease) was incubated for 15
281 minutes at 30°C. Post incubation, 1 μ l sodium nitroprusside 0.005% (w/v) and 45 μ l
282 phenol reagent (phenol 1% (w/v) was added, following the addition of alkali reagent (70
283 μ l; 0.5% NaOH and 0.1% NaOCl) and incubation at 30°C for 50 minutes. The reaction
284 controls: positive control (thiourea); and blank (solution without CuO-NPs) were taken
285 in parallel. The optical density was measured at 630 nm and % inhibition of urease was
286 evaluated by following equation (Eq. 3):

$$287 \quad \% \text{ Enzyme inhibition} = OD(b) - \frac{OD(s)}{OD(b)} \times 100 \text{ ----- (Eq. 3)}$$

288 where OD (b) stands for "blank" and OD (s) for "test sample value."

289 **2.4.5 Lipase inhibition assay**

290 The lipase inhibition assay was ascertained following the slight modified
291 procedure of [63]. The enzyme lipase (10 mg ml⁻¹) in aqueous state was subjected to
292 vortex (6,000 rpm; 5 min.) and the resultant supernatant was rescued. The reaction
293 mixture [Tris buffer (350 μ l; 100 mM; pH 8.2), 150 μ l lipase and CuO-NPs (50 μ l)] was
294 taken and mixed with substrate (olive oil; 450 μ l) in order to initiate the reaction and
295 incubated at 37°C for 120 min. Post incubation, the solution was centrifuged (16,000 rpm;
296 5 min.) and the optical density was read at 400 nm by taking 200 μ l of the resulting
297 supernatant. The reaction controls: blank [buffer (400 μ l), lipase (150 μ l), and substrate

298 (450 µl)] and positive control (orlistat) were running parallel. The percent inhibition of
299 enzyme was evaluated by equation (Eq. 3).

300 **2.5 Antioxidant activities of biosynthesized CuO-NPs**

301 **2.5.1 Free radical scavenging assay (FRSA)**

302 The DPPH (2,2-diphenyl 1-picrylhydrazyl) assay was performed for the
303 assessment of free radical scavenging potential of CuO-NPs [64]. Briefly, 10 µl CuO-
304 NPs+ 190 µL DPPH reagent were mixed and kept for 30 min at 37°C. Ascorbic acid was
305 act as positive control. The absorbance of reaction solution was recorded at 515 nm and
306 the following equation (Eq. 4) was used to estimate the scavenging activity:

$$307 \quad \% \textit{ Scavenging} = \left(1 - \frac{AE}{AD}\right) \times 100 \quad \text{----- (Eq. 4)}$$

308 where AE directs absorbance of test sample solution and AD denotes negative control.

309 **2.5.2 Total antioxidant capacity (TAC)**

310 The total antioxidant capacity of CuO-NPs was quantified by using
311 phosphomolybdenum method [65]. Briefly, 900 µl phosphomolybdenum reagent
312 [sulphuric acid (0.6 M), ammonium molybdate (4 mM), and sodium phosphate (28
313 mM)]+ 100 µl CuO-NPs was mixed and kept for 90 min at 95°C. Post incubation, the
314 absorbance of the reaction mixture (volume 200 µl) was read at 695 nm. The antioxidant
315 potency was ascertained as the amount of ascorbic acid equals to ascorbic acid per mg
316 of test sample (mg AAE/mg).The positive reference employed was ascorbic acid.

317 **2.5.3 Total reducing power (TRP)**

318 The total reducing power of CuO-NPs was investigated by potassium
319 ferricyanide based assay [65]. Iron, as reducing agent, was used for the quantification of

320 total reducing power. The reaction mixture: 40 μ l CuO-NPs + phosphate buffer (400 μ l,
321 0.2 mol/l, pH 6.6) + aqueous potassium ferricyanide (1%) was kept at 45°C for 20 min.
322 Post incubation, aqueous trichloroacetic acid (400 μ l; 10%) was added and mixed in the
323 resulting mixture; centrifuged at 3000 rpm for 10 min. The resultant supernatant
324 (volume 500 μ l) was added with equal volumes of 100 μ l aqueous FeCl₃ (0.1%) and
325 sterile distilled water. The absorbance (630 nm) was read and the outcomes were
326 quantified as mg AAE/mg. The reaction controls: positive control (ascorbic acid) and
327 blank (DMSO) were run in parallel.

328 **2.5.4 ABTS antioxidant assay**

329 The ABTS assay was investigated by following the protocols of [66]. The reaction
330 mixture [equal proportions of 7mM ABTS salt and potassium persulphate (2.5 mM)]
331 was kept under dark conditions for 14-16 h. Prior to the addition of CuO-NPs, the
332 absorbance (734 nm) was read and adjusted to 0.7. The variable concentrations of CuO-
333 NPs were then added to the reaction mixture and kept for 15 min at room temperature
334 under dark conditions. The antioxidant effect has been detected in TEAC and the
335 absorption was measured at 734 nm (trolox C equivalent antioxidant capacity, mM).

336 **2.5.5 FRAP (ferric reducing antioxidant power) assay**

337 The ferric reducing power was investigated as developed by [67]. 10 μ l CuO-NPs
338 was added to 190 μ l FRAP solution [TPTZ (2,4,6-tri(2-pyridyl)-s-triazine; 10 mM);
339 acetate buffer (300 mM; pH 3.6); FeCl₃.6H₂O (ferric chloride hexahydrate; 20 mM) in the
340 ratio 10 : 1 : 1 (v/v/v)] and kept for 15 min. at room temperature. The O.D (630 nm) was
341 recorded and the reducing antioxidant effect was determined as TEAC.

342 **2.5.6 Nitric oxide scavenging activity**

343 Nitric oxide (NO₂) scavenging capacity was measured by the procedure of [68].
344 Briefly, different CuO-NPs concentrations (20–100µg/ml) were mixed with sodium
345 nitroprusside solution (10 mM) and kept for 2.5 h at 25°C. Following incubation, the
346 reaction solution (0.25 ml) was mixed with sulfanilic acid and n-1-naphthyl indicator
347 (0.5%; 0.5 ml) and kept at 25°C for 30 min. The absorbance was read at 540 nm and the %
348 scavenging activity was evaluated by the following equation (Eq. 5):

349
$$\text{Scavenging activity \%} = \frac{\text{Abs (control)} - \text{Abs (sample)}}{\text{Abs (control)}} \times 100 \text{ ----- (Eq. 5)}$$

350 where Abs control and Abs sample stand for the relative absorption of the control and
351 sample.

352 **2.5.7 Hydrogen peroxide radical scavenging (H₂O₂) assay**

353 The H₂O₂ scavenging capacity of CuO-NPs was ascertained by the protocol of
354 [69]. The reaction solution consisted of hydrogen peroxide (40 mM) in phosphate buffer
355 (50 mM, pH 7.4) was prepared. The H₂O₂ concentration was determined at wavelength
356 230 nm. The resulting combination was mixed with aqueous CuO-NPs (20–100 µg/ml)
357 and allowed to stand at room temperature for 30 min. The reaction solution was
358 measured at 230 nm in comparison to a blank solution (phosphate buffer without
359 hydrogen peroxide), and the equation was used to determine the percentage of
360 hydrogen peroxide scavenging (Eq. 5).

361 **2.6 Measurement of peroxidase-like activity of CuO-NPs**

362 The POD (peroxidase) activity was ascertained as described by [70]. Briefly, the
363 reaction mixture: 140 µl NaAc–HAc buffer (0.2 M, pH 4.0) + 20 µl CuO-NPs were mixed
364 thoroughly with the subsequent addition of freshly prepared H₂O₂(6 mM) and freshly
365 prepared TMB (3 mM, 20 µl). The absorbance (652 nm) was read and the reaction

366 combination (with no test sample) was taken as control. The enzymatic activity was
367 determined by using equation (Eq. 6):

368
$$A = ELC \text{ ----- (Eq. 6)}$$

369 where A denotes the sample absorption value, C the enzyme content (measured in
370 millimolars per milligram), E the extinction coefficient, and L the wall length,
371 correspondingly.

372 **2.7 Detection of reactive oxygen/nitrogen species**

373 The generation of reactive species (ROS and RNS) by CuO-NPs was reported by
374 using fluorescent dye DHR-123 (dihydrorhodamine-123) [67]. Yeast cells, in existence of
375 CuO-NPs and control (DMSO), was incubated for overnight under dark at 30°C for 10
376 min. Post incubation, the cells were cleaned with PBS thrice and re-suspended in 0.4 μM
377 DHR-123 dissolved in PBS. The fluorescence wavelengths $\lambda_{ex} = 505 \text{ nm}$, $\lambda_{em} = 535 \text{ nm}$
378 were used to detect the fluorescence by BioRad Versa Fluor Fluorimeter.

379 **2.8. Metal chelating activity**

380 The metal ion chelating property of SH assisted CuO-NPs were quantified. The
381 reaction mixture consisting of: FeSO₄ (1ml) + CuO-NPs (20-100μg/ ml) + solution of 2,2'-
382 bipyridyl (1ml) and Tris- HCl buffer (pH 7.4) + mixture of ethanol and hydroxyl amine-
383 HCl. The reaction mixture (5ml) was maintained for 10 min at room temperature. The
384 O.D values was read at 522 nm and the ion chelating activity was measured by Eq.(5)
385 [71].

386

387 **2.9 Assessment of Antibacterial activity of CuO-NPs**

388 **2.9.1. Maintenance of pathogenic strains**

389 Two bacterial pathogens, namely, *Escherichia coli* and *Staphylococcus aureus* were
390 sub-cultured periodically on MHA and maintained as culture stock in form of 10%
391 glycerol stocks (-20°C) and slants at (4°C).

392 **2.9.2. Minimal Inhibitory Concentration (MIC) and Minimal Bactericidal** 393 **Concentration (MBC) of CuO-NPs**

394 For evaluation of MIC, broth micro-dilution technique was employed [1, 72]. The
395 variable concentrations of CuO-NPs (20-100µg/ml) were tested; maintained for 24 hat
396 37°C along with control tubes. The optical density was measured at 620 nm. For
397 assessment of MBC, aliquots (20 µl) from MIC tubes assay were seeded, cultured on NA
398 medium followed by incubated for 24h at 37°C [3, 73].

399 **2.9.3. Antibacterial activity of CuO-NPs**

400 The bactericidal effects of CuO-NPs was performed by using agar well diffusion
401 technique [1, 74, 75] against human pathogens (*E. coli* and *S. aureus*). The bacterial
402 culture (0.1 ml; cell density 2×10^8 CFU/ml) were lawn spread uniformly on MHA media.
403 Equal sized wells were made and variable concentrations of CuO-NPs (20, 60, 80, and
404 100µg/ml) were added to the former and stored at 37°C for 24 h. The antibiotic cefixime
405 act as positive control and the size of zone of inhibition (ZOI) was calculated by
406 antimicrobial zone measurement scale (Hi-Media, India).

407 **2.9.4. Anti-biofilm potential of CuO-NPs**

408 The anti-biofilm efficacy of CuO-NPs was analyzed by employing CV (crystal
409 violet) assay [1]. Starter cultures (100 µl; cell density $\sim 10^8$ cells/ml) of *S. aureus* and *E.*
410 *coli*, grown overnight in NB, were seeded into 96-well microtitre plate. A 100 µl culture
411 medium + variable CuO-NPs concentrations (100 µl; 20–100µg/ml) was dropped to the
412 respective wells along with a parallel set of untreated culture run as control followed by

413 cultivation for 24 h at 37°C. The remaining loosely bound cells were washed thrice with
414 PBS (phosphate buffer saline) + autoclaved distilled water (1:1). The CV solution (0.25%,
415 200µl) was added followed by incubation for 30 min at 37°C. The unbound CV was
416 washed with PBS + autoclaved distilled water. The bound CV-bacterial cells were
417 dissolved in ethyl alcohol (95%; 250 µl) and the absorbance read at 620 nm using ELISA
418 reader.

419

420 **2.10. DNA cleavage assay**

421 The CuO-NPs treated vector pBR322 DNA was examined as described by [76].
422 Aliquots (50 µl) of SH and CuO-NPs (20, 60, 100 µg/ml) solutions were separately
423 added to vector DNA (1µl; 0.5 µg/ml) in TE buffer (0.1 mM EDTA, 10 mM Tris-HCl, pH
424 7.4) followed by incubation at 37°C for 24 h under dark. Consequently, gel
425 electrophoresis (1% agarose gel) was run by using 20 µl copper acetate and CuO-NPs-
426 bacterial DNA mixtures each and viewed using UV light trans-illuminator equipped gel
427 documentation system.

428 **2.11. Mechanism of action of CuO-NPs on treated bacterial cells**

429 **2.11.1. Protein leakage assay**

430 The estimation of cellular protein leakage was ascertained by previously
431 developed protocol of [77]. The CuO-NPs (MIC concentration) treated bacterial cells
432 were incubated for fixed time intervals of 3h and 6h and then centrifuged at 6000 rpm
433 for 15 min. For each ensuing sample, the Bradford reagent (800 µl) + supernatant (200 µl)
434 were mixed; followed by incubation for 10 min at room temperature. The protein BSA
435 served as standard for the measurement of optical density (λ 595 nm).

436 **2.11.2. Nucleic acid (NA) leakage assay**

437 The quantification of NA leakage was ascertained by the protocol of [78].
438 Aliquots of CuO-NPs (MIC concentration) treated bacterial cultures were incubated for
439 fixed time intervals of 3h and 6h followed by filtration by Millex-GS syringe filters
440 (Millex-GS, Spain) using dimension: diameter 25 mm; pore size 0.2 µm. The values of
441 absorbance were measured at 260 nm.

442 **2.12. Brine shrimp lethality assay for cytotoxicity test**

443 The precursive cytotoxicity of CuO-NPs was determined by employing brine
444 shrimp lethality assay [79]. The medium comprising of artificial seawater (34 g sea salt +
445 1.0 liter sterile distilled water under incessant stirring) was used for hatching eggs of
446 *Artemia salina* (brine shrimp) between 28±2.0°C. After egg hatching, 5 ml brine was
447 added to the test CuO-NPs concentrations. Post 2 days, hatched shrimps were
448 transferred to the test CuO-NPs concentrations (15 shrimps/concentration). After 24 h,
449 the number of surviving shrimps was recorded and the percentage viability was
450 calculated based on the following method (Eq. 7):

$$451 \quad \text{Percentage viability} = \frac{\text{control} - \text{test}}{\text{control}} \times 100 \text{ ----- (Eq. 7)}$$

452 **2.13. Dye degradation and kinetics study**

453 The degradation of azo-dyes (RR195 and RY145) was calculated using optimized
454 SH-assisted CuO-NPs as nanocatalysts using NaBH₄ [21]. For experiment, dye (10 mg
455 each) + 1.0 liter sterile distilled water were mixed; accounting stock solutions for two
456 separate simulated wastewater samples. The CuO-NPs (20 ml) were added and mixed
457 with 10 ml as-prepared simulated wastewater and 100 ml aqueous NaBH₄ solution
458 (0.1mol/l). The resulting solution was well mixed by manual shaking, and the UV-Vis
459 absorption spectra were promptly read at room temperature. The catalytic degradation

460 was measured by recording time-dependent change in the absorbance. A common
461 equation (Eq. 8) was used to measure the amount of dye degradation (D%):

$$462 \quad D\% = \frac{(A_0 - A_t)}{A_0} \times 100 \text{ ----- (Eq. 8)}$$

463 where A_t denotes absorption at a specific time and A_0 denotes starting absorbance. (t).

464 The rate constant was evaluated by typical kinetic equation (Eq. 9):

$$465 \quad \ln \left(\frac{A_t}{A_0} \right) = -kt \text{ ----- (Eq. 9)}$$

466 where k corresponds to the kinetic degree constant, t indicates reduction time, A_0 was
467 the measure of initial spectrum, and A_t was the measure of absorbance of dyes at time
468 t .

469 **2.14. Statistical analysis**

470 All investigations were performed in triplicates and the data were interpreted as
471 mean \pm S.D. calculated by using SPSS (Version 7.5.1, USA). The results of inhibition
472 assays; peroxidase and ROS/RNS activity were evaluated by One-way ANOVA
473 (analysis of variance) followed by unpaired Bonferroni test. The p value <0.05 indicated
474 the arithmetical significance of results.

475 **3. Results and Discussion**

476 The current study employs sodium hyaluronate as stabilizing and reducing
477 agent in the synthesis of copper oxide nanoparticles. In study, the sodium hyaluronate
478 was chosen as the base material owing to its attributes of naturally occurring polymer
479 that gels in the presence of a cross-linker sans the need for organic solvents or extremely
480 high temperatures. This function conveniently prevents the loss or destruction of labile
481 medications [80, 81]. Also, the molecules of hyaluronate are biocompatible and
482 encourage interaction of biological cues with particular cellular receptors [82].

483 **3.1. Synthesis and optimization of SH- assisted CuO-NPs**

484 The formation of SH-CuONPs was preliminary inveterate by the visual color
485 shifted of the reaction mixture. An aqueous solution of SH is colorless, while the
486 solution of copper acetate [Cu(OAc)₂] was found to be blue colored. However, the color
487 of the reaction mixture changed under thermal heating, depending upon the reaction
488 parameters. The coupled oscillation of free electron conduction, induced by LSPR
489 representing the production of CuO-NPs, is responsible for the development of vivid
490 colour [3, 83]. The size and form of the colloid's particle were linked to the variations in
491 colour as the literature states that colour change from bluish green to grayish black are
492 suggestive of the formation of colloidal CuO-NPs at the nanoscale [3]. The spectroscopic
493 analysis of the colloid reaction mixture validated the development of CuO-NPs (Fig.
494 1a). The absorption peak at 244 nm of copper acetate was recorded primarily due to
495 LMCT transition (ligand-to-metal-charge-transfer) of AcO⁻ ions and d-d transition of
496 Cu²⁺ ions. On the other hand, no absorptive peak was exhibited by SH under observed
497 wavelength range. However, heating at ambient conditions caused the dissipation of
498 UV-Visible absorption peak of Cu(OAc)₂ at 244 nm indicating the reduction of Cu²⁺ into
499 Cu⁰ [83]. The generation of CuO-NPs was exhibited by the concurrent peak appearance
500 at 575 nm and a strong plasmonic peak band between 550 and 590 nm (depending on
501 size and shape of the particle) [84, 85]. The controlled and tailored characteristics of
502 synthesized CuO-NPs require the determination of ideal concentration of
503 stabilizing/reducing agents. To understand and quantify the effects of different dosages
504 of stabilizing/reducing agents, the CuO-NPs were synthesized through the reduction of
505 Cu²⁺ to Cu⁰ by adjusting the SH concentration from 0.05-0.25% (w/v) while keeping
506 other parameters constant (Fig. 1b). Further, it was observed that no apparent
507 absorption was found between 550 and 590 nm at 0.05%SH inferring no appreciable
508 effect on the reduction of Cu²⁺ ions. However, as the concentration of SH was raised to

509 0.10%, a reduction peak at 533 nm began to rise, indicating the beginning of reduction
510 process. A strong and sharp peak was exhibited by increasing the SH concentration
511 further to 0.15%. Further, a considerable red shift from 550 to 650 nm was observed,
512 even though the reaction's maximum absorption intensity was obtained at 0.20% SH,
513 which may be due to the increase in the size of the nanoparticles [86]. Also, when SH
514 concentration was increased further to 0.25%, the intensity of the absorption
515 dramatically decreased, resulting in an additional red shift of 610 nm. Here, rather than
516 the interactive effects with saturated Cu^{2+} ions, the increased concentration of SH caused
517 the contact between functional groups. As a result, nanoparticles changed into clusters
518 or CuO-hydro-complexes rather than particles [87]. As a result, the optimal
519 concentration for this reduction process was found to be 0.15% SH.

520 A suitable amount of reaction incubation time (t) is necessary to reach the yield
521 point of reduction under the conditions of complete nucleation and the resulting
522 stability of CuO-NPs. To regulate the time of equilibrium for particle development and
523 stability, the spectrophotometric investigation of the reaction kinetics of particle
524 formation was performed (Fig. 1c). No obvious peaks were recorded during the first 20
525 minutes of the reaction, thereby indicative of the absence of CuO-NPs synthesis. A faint
526 and broad peak with little to no absorption intensity was observed at 535 nm after 30
527 minutes of reaction. Also, there was a notable rise in the intensity of peak absorption
528 and sharpness and strength of the band after another 10 min of reaction time. Although,
529 the reaction increased the absorption intensity over a 50-min time period, the band
530 widened and experienced a considerable red shift to 610 nm, suggesting instability in
531 the formed nanoparticles. The growth and stabilization of CuO-NPs was fully achieved
532 within 40 min of the reaction. It is necessary to carry out the synthesis reaction at an
533 appropriate temperature (T) in order to obtain the specific size/shape of nanoparticles.

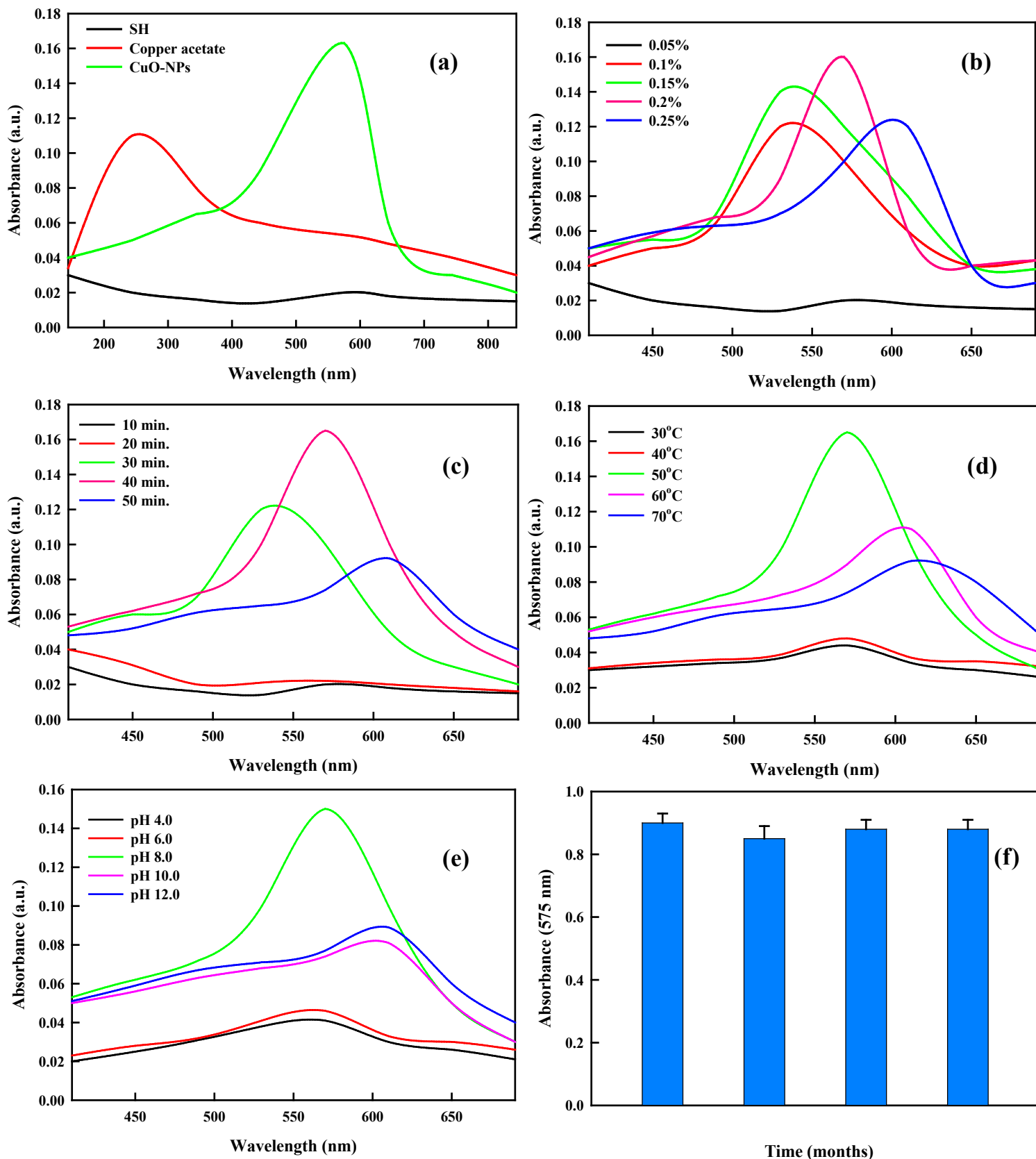
534 As a result, the temperature range between 30-70°C was used for the temperature-
535 dependent synthesis of CuO-NPs (Fig. 1d). The reaction was conducted between 30 and
536 70°C and a strong noticeable absorption band was seen at 50°C confirming the formation
537 of CuO-NPs. The results exhibited a negative association between temperature and
538 particle size, with further increase at 70°C showing no increase in absorption intensity
539 or sharpening of absorption band but causing disappearance and widening of
540 absorption peak [52, 88]. The optimized temperature for the production of SH assisted
541 CuO-NPs was found to be 50°C. Also, the pH of the reaction also plays an imperative
542 role in the control of growth and properties of synthesized nanoparticles. The
543 biosynthesis of SH-CuONPs was undertaken at variable pH (4–12) (Fig. 1e). The pH-
544 dependent wavelength absorptive spectra exhibited no promising visible peaks at both
545 acidic (pH = 4–6) and basic (pH = 10–12). However, the reduction of Cu²⁺ ions and
546 subsequent production of CuO-NPs were indicated by a distinct and strong absorption
547 peak at near neutral to slight basic pH 8. A broad absorption band and steady
548 absorption intensity were the consequences of the reaction under both acidic and basic
549 extremities of the reaction media.

550 The nanoparticles mediated biological activities, particularly their antimicrobial
551 effects, are influenced by a number of factors, including their surface charge, capping
552 agent, ionic strength, pH, size morphology and shape [89]. The functionality of metal
553 nanoparticles for different applications is further enhanced by adjusting their size and
554 shape. During the optimization of synthetic procedures of nanoparticles by biological
555 pathway, the precise control of these parameters may be crucial. By altering the
556 medium's pH, it is possible to influence the shape and size of nanoparticles, with an
557 acid pH resulting in the generation of large NPs. This is because there are more
558 functional groups available at higher pH ranges than at lower pH ranges, making them

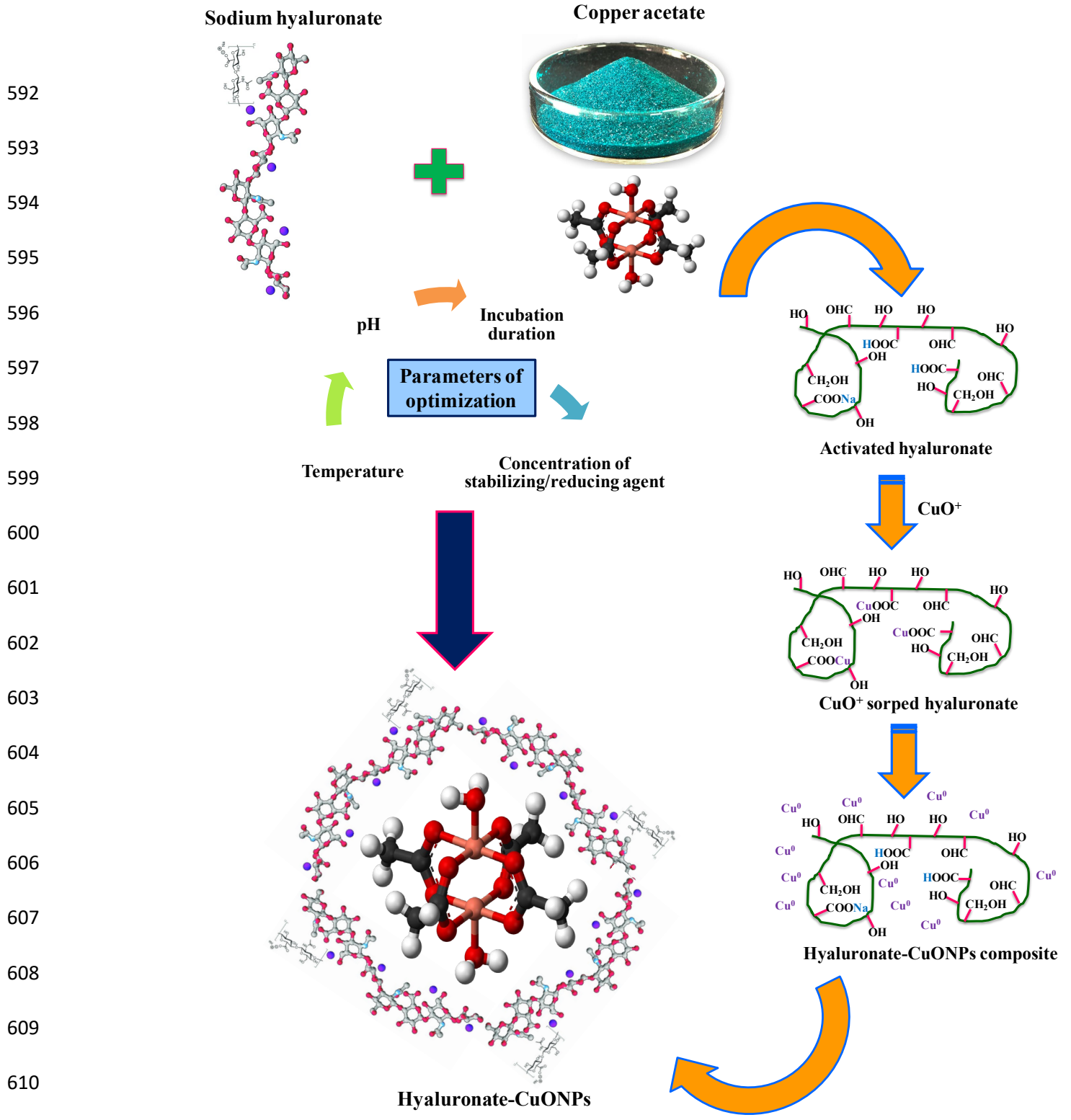
559 more accessible for nucleation [90]. Besides pH, the solution concentration also
560 influences the size and form of biosynthesized nanoparticles. A quick change in the
561 color of the reaction mixture is the primary indicator that the reaction's time is
562 important in the reduction of nanoparticles and their size. This time frame can
563 range from minutes to hours. The shape, size, and yield of nanoparticles are also
564 influenced by the reaction temperature, which is another crucial factor in the
565 biosynthesis of nanoparticles [89].

566 Polysaccharides are essential compounds for the creation of multi-facet nano-
567 based materials since they serve as the foundation for fibers, coatings, and stabilizing
568 agents [91]. They are renewable resources that have undergone extensive research
569 owing to their biodegradability, biocompatibility, and variety of biological activity [92,
570 93]. They are organic macromolecules made up of covalently bonded monosaccharide
571 units connected by polymer chains [94]. Today, a multitude of polysaccharides are
572 obtained through extraction from natural sources such as microorganisms, algae, plants,
573 animals [95]. The mechanism of formation of polysaccharides units (here, hyaluronate;
574 Fig. 2) assisted metal based nanoparticles (here, CuO-NPs) can be explained as follows:
575 Metal ions are hosted by the units of polysaccharides by non-covalent bonding
576 (sorption). By changing the order of free energy (heating), the metallic precursor is
577 subsequently reduced to a zero-valent state, initiating the process of nucleation and
578 formation of nanocrystal. The metal nanoparticles are stabilized by the rise in
579 temperature, which also enables control over their growth kinetics and shape. In
580 contrast to top-down synthesis, when the initial materials are shrunk down through
581 chemical, thermal, or mechanical processes, this sort of self-assembling (bottom-up)
582 synthetic process is favored. These processes could cause the nanoparticles to oxidize
583 unintentionally, changing their surface chemistry and/or physical characteristics.

584 Furthermore, sans an external stimulation like a pH shift, the stabilized metal based
585 nanoparticles do not readily leach out of the integrated metal ion-
586 polysaccharide complex. Since most polysaccharides are sensitive to pH changes, they
587 are frequently used in polysaccharide-based systems for controlled drug delivery [96,
588 97].



590 **Fig.1** (a) UV-Vis spectra of SH, copper acetate and CuO-NPs. Effect of (b) SH concentration, (c)
 591 reaction time, (d) reaction temperature, (e) pH, (f) stability over time



612 **Fig. 2** Mechanism of hyaluronate assisted CuO-NPs synthesis

613

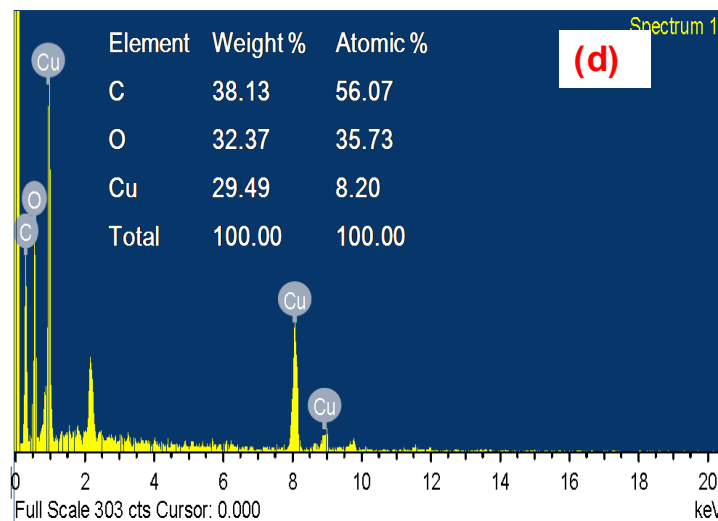
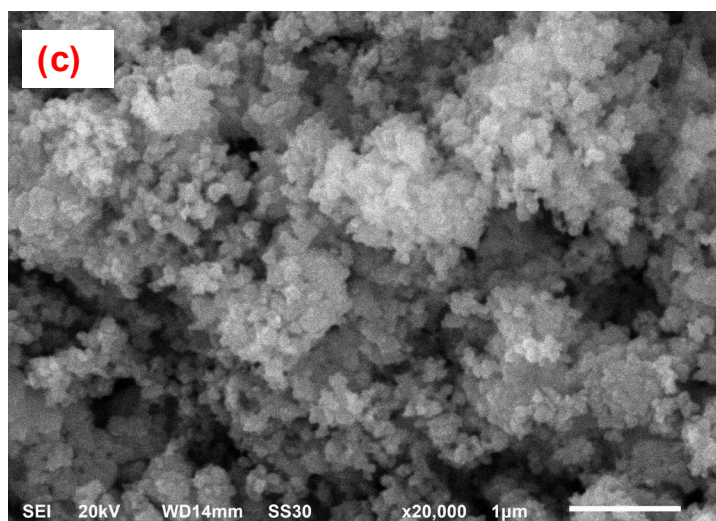
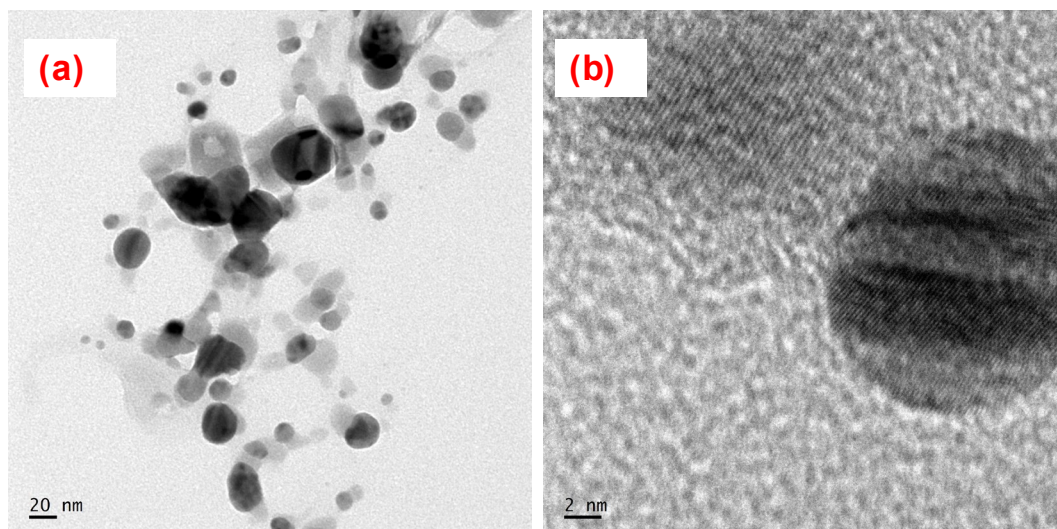
614 **3.2. Characterization of fabricated CuO-NPs**

615 For the biosynthesis of SH assisted CuO-NPs in the current investigation, a
616 matrix of sodium hyaluronate was used. After washing, drying, and annealing, a fine
617 black powder of CuO-NPs was produced, and stored till further processing for
618 morphological, physiochemical, and biological experimentations. The initial TEM
619 analysis of the morphology and size of CuO-NPs exhibited successful synthesis of
620 polydispersed CuO-NPs with a particle size of 17.4 ± 1.3 nm (Fig. 3a and b). The
621 observation also demonstrated the oval and spherical form of SH-produced CuO-NPs.
622 The high-resolution TEM was used to capture a section of a single particle,
623 demonstrating highly crystalline surface of CuO-NPs. Additionally, SEM was used to
624 observe the solid-state particles (Fig. 3c). It revealed that CuO-NPs was equally
625 distributed throughout the SH composite with no aggregation, demonstrating the
626 ensnarement of CuO-NPs in SH molecules conferring stability. Furthermore, the EDX
627 microanalysis showed the presence of copper component (29.49%) in nano form rather
628 than copper derived compounds (Fig. 3d). The purity and structural morphology of
629 CuO-NPs was shown by X-ray diffraction pattern found with diffraction angles ranging
630 from 10 to 70. Strong peaks at 23.44, 31.18, 34.38, 37.58, 38.80, 43.60, 47.65, 57.24, 60.43,
631 65.11 and 66.95 corresponding to the miller indices (100), (-111), (002), (-102), (-211), (-
632 112), (012), (-221), (020), (-312) and (021) confirmed with JCPDS file no. 048-1548 [98]
633 (Fig. 4a). The Debye Scherrer equation exhibited the crystalline monoclinic phase of
634 CuO-NPs. Similar results were also reported in the studies of [3, 57, 99, 100]. It was
635 important to note that the crystal size calculated by the XRD using the Scherrer
636 equation (16.67 nm) was relatively smaller than the particle size discovered in TEM
637 (17.4 ± 1.3 nm). The size of twinned particles with multiple diffraction domains is lower

638 than the diameter measured by XRD analysis, which is a measure of single-crystal
639 particles and could be the cause of the size discrepancy. The TEM image (Fig. 2b)
640 substantiated the theory and clearly demonstrated that some particles were >16 nm
641 with grain twinning and boundary [101].

642 The FTIR chemical analysis was used to understand the interaction between SH
643 and copper oxide ions (Fig. 4b). The primary peaks of aqueous SH identified were: 3370
644 cm^{-1} (-OH stretch), 1412 cm^{-1} (C-H stretch), and 1082 cm^{-1} (C-O-C). The CuO-NPs had
645 comparable spectral morphologies, but their peak positions had a tiny shift to the lower
646 bands (3579, 3482, and 1120 cm^{-1} , respectively) as a result of conformational changes
647 that were caused by CuO-NPs in SH chains through dipole-dipole interactions and H-
648 bonding. Also, a prominent SH peak (indicated by a rectangular area) at 1405 cm^{-1} (C-O-
649 C) was totally absent, while the peak at 1157 cm^{-1} sharpened as a result of the
650 vibrational stretch of (NH)C=O. Therefore, it is clear that the interaction between
651 functional groups of SH, particularly -OH, -NH(C)=O, -COOH groups, and CuO-NPs
652 enabled reduction of Cu^{2+} ion. These interactions were suggestive of the SH
653 macromolecule capping and stabilizing CuO-NPs.

654
655
656
657
658
659
660



661 **Fig.2** Electron microscopic analyses of CuONPs. (A) TEM image at 20 nm; (B) TEM image at 2
662 nm; (C) SEM micrograph at 20000X and (D) EDS spectrum displays the % of C, O and Cu
663 elements in SH-CuONPs.

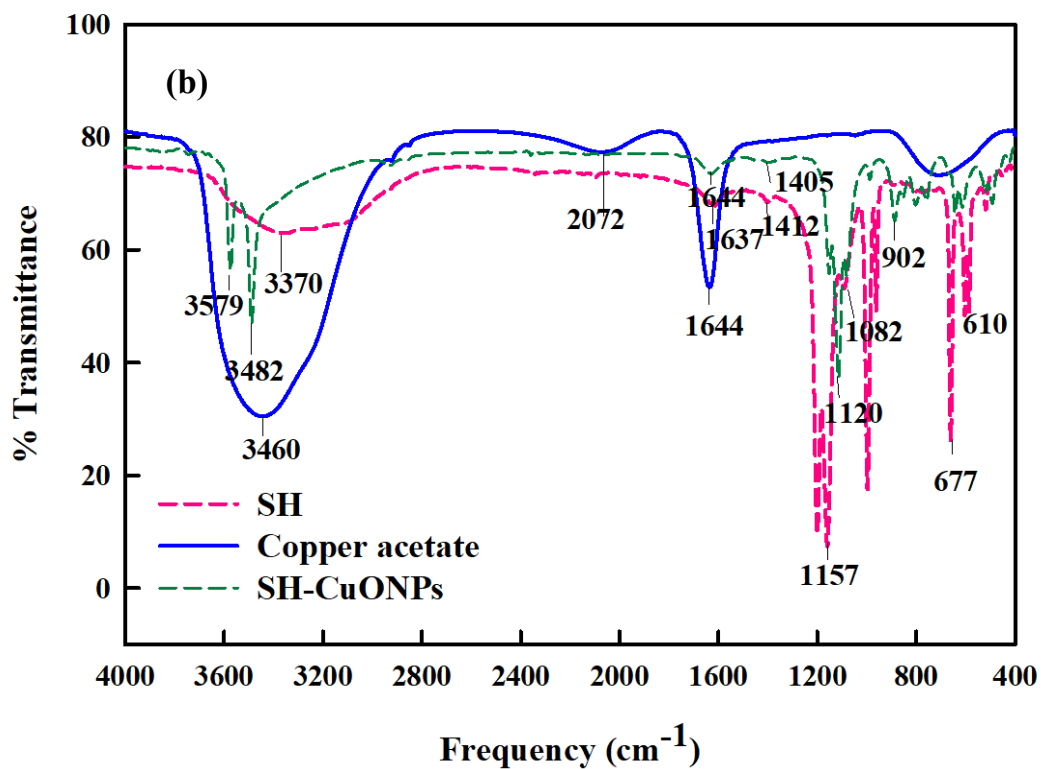
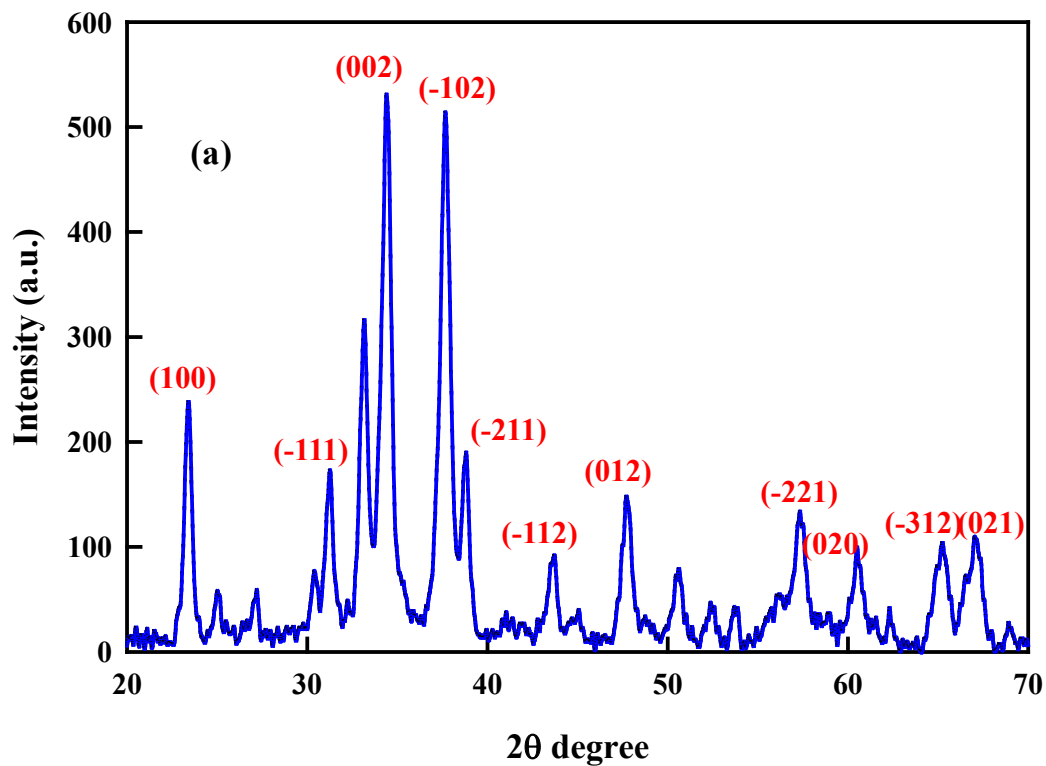


Fig.3 Physicochemical characterization of CuONPs. (a) X-ray diffraction (XRD) (b) FTIR analysis

685

686 3.3. Biological activities of CuO-NPs

687 Diabetes and its complications are a severe and common source of illness and
688 mortality all over the world. A metabolic disease known as diabetes melitus (DM) is
689 characterized by chronic hyperglycemia induced by cellular insensitivity to insulin or
690 decreased insulin production [102]. Some phyto-based chemicals have been reported as
691 inhibitors of starch hydrolysis and are considered an appealing contender in the
692 treatment of diabetes mellitus in addition to anti-diabetic medications used in the
693 regulation of post-prandial hyperglycaemia. To assess the ability of SH assisted CuO-
694 NPs in the inhibition of enzyme α -amylase; the former was subjected to experimental
695 assay. The results revealed that biosynthesized CuO-NPs showed a satisfactorily high
696 amount of α -amylase and α -glucosidase enzyme inhibitions ($72\pm 1.2\%$ and $70\pm 2.1\%$), as
697 compared to that of SH at $100\ \mu\text{g/ml}$ (Fig. 5a, b). According to our findings, the SH
698 assisted CuO-NPs exhibited significant enzymatic inhibitory activity which were
699 similar to the reports of [43, 100, 103]. Also, the graphic representation of HbA1c assay
700 results (Fig. 5c) inferred a dose-dependent inhibition. It was clearly explained as a
701 concentration-dependent reduction in the % of inhibition at various concentrations of
702 biosynthesized CuO-NPs ($20\text{-}100\ \mu\text{g/ml}$). The maximum concentration ($100\ \mu\text{g/ml}$) of
703 CuO-NPs and metformin, exhibited maximum inhibitions of $70\pm 2.1\%$ and $86\pm 1.4\%$,
704 respectively, whereas the minimum concentration ($20\ \mu\text{g/ml}$) of CuO-NPs and
705 metformin exhibited the least inhibitory value. There are a number of causes for α -
706 amylase inhibitory potential of medicinal plants, such as concentration of fibre, fibre
707 cocooned encapsulation of enzyme and starch, and inhibitors on fibre surface, resulting
708 in the reliable adsorption of enzyme α -amylase onto the surface of fibre and reduced
709 starch accessibility to enzyme, resulting in the diminished activity of α -amylase [104].

710 By delaying carbohydrate digestion and lengthening the overall time of carbohydrate
711 digestion, α -glycosidase inhibitors can aid in lowering post-meal blood sugar levels.
712 The inhibitors such as miglitol, vogomibose, and acarbose have been utilized as first-
713 line therapies for diabetes type 2 in the clinical context. Unfortunately, these therapies
714 may have unwanted consequences like bloating, stomach pain, and diarrhea. Therefore,
715 for the proper management of diabetic diseases, the development of safe and efficient
716 enzyme inhibitors is necessary [105, 106].

717 A biologically active enzyme called urease breakdown urea into carbon dioxide
718 and ammonia. Urea is widely distributed in biologically active soil because many
719 microorganisms metabolize it through the enzymatic action of urease [107]. The SH-
720 assisted CuO-NPs displayed outstanding urease inhibitory potential, as evidenced by
721 the urease inhibitory assay results, which showed % inhibition of $68 \pm 2.1\%$ compared to
722 thiourea at $100 \mu\text{g/ml}$ (Fig. 5d). During biosynthetic process, the functional groups
723 attached to CuO-NPs may be responsible for this inhibitory action. Further, the
724 triglycerides are hydrolyzed into fatty acids and glycerol molecules by a class of
725 enzymes called lipases. These fat-splitting enzymes can be found in the pancreatic
726 secretions, stomach juices, and blood [108]. In the present study, SH-assisted CuO-NPs
727 exhibited high potential for inhibiting enzymatic activity of enzyme lipases. At 100
728 $\mu\text{g/ml}$, CuO-NPs demonstrated a percent inhibition of $70 \pm 2.3\%$ (Fig. 5e). The biological
729 molecules conjugated to CuO-NPs during the biosynthesis process may be a plausible
730 factor contributing in the inhibitory effect. This inhibitory property may be brought on
731 by the various biological molecular species and functional groups like -OH (hydroxyl)
732 and C=O (carbonyl) groups [107, 109].

733 Free radicals are molecules devoid of full electron shell, which speeds up a
734 chemical process compared to other molecules. Oxygen (O₂) is the most significant free
735 radical in physiological systems. Radiation causes O₂ to transfer electrons from other
736 molecules, causing the destruction of DNA and other molecules [110-112]. Some of
737 these modifications lead to illness such as cancer, diabetes, heart issues, and muscle
738 failure. Antioxidants sweep away free radicals like a broom, repairing damaged cells as
739 demonstrated by the studies of [113, 114]. The antioxidant assays of FRAS, TRP, TAC,
740 FRAP, and ABTS are used to examine the antioxidant capacity of CuO-NPs. The FRAS
741 assay was analyzed by using DPPH molecule. The colour of the stable free radical
742 DPPH is purple with a significant absorption maximum observable at 517 nm. The free
743 radical in the DPPH is paired off in the presence of an antioxidant, which reduces the
744 absorbance and colour intensity. The DPPH technique is quick, easy, and affordable to
745 test the antioxidant properties of compounds and is frequently used to assess their
746 capacity to function as hydrogen providers and free-radical scavengers. The DPPH test
747 depends on DPPH, a stabilized free radical, being eliminated. In fact, DPPH is a stable
748 free-radical molecule that has a dark colour and crystalline structure. It is a widely
749 recognized antioxidant and radical test in which the DPPH radical initially exhibits a
750 dark purple tint in solution; however, after reduction and transformation into DPPH-H,
751 it becomes colorless or light yellow [115]. The CuO-NPs reduces DPPH radicals by the
752 transference of an electron or proton. In present study, the amount of DPPH-scavenging
753 activity rose linearly from 20-100 µg/ml of CuO-NPs concentration, exhibiting 70±2.3%
754 scavenging activity at 100 µg/ml (Fig. 6a). The CuO-NPs exhibited a high TAC value of
755 85±0.26 µg AAE/mg (Fig. 6b). The TRP value of CuO-NPs is larger than that of
756 hylauronate solution at 76±0.35 µg AAE/mg (Fig. 6c). Additionally, the synthesized
757 CuO-NPs had a high ABTS value (400 µM TEAC) and a high FRAP value (423 µM

758 TEAC) (Fig. 6d and e). Further, the transition metal ions, particularly Fe^{2+} , can hasten
759 lipid peroxidation by (i) initiating fenton reaction or (ii) by breaking down lipid
760 hydroperoxide into alkoxy and peroxy radicals triggering a chain reaction. In the
761 study, the treatment of CuO-NPs resulted in an increase of 33% in the metal chelation
762 (Fig. 6f).

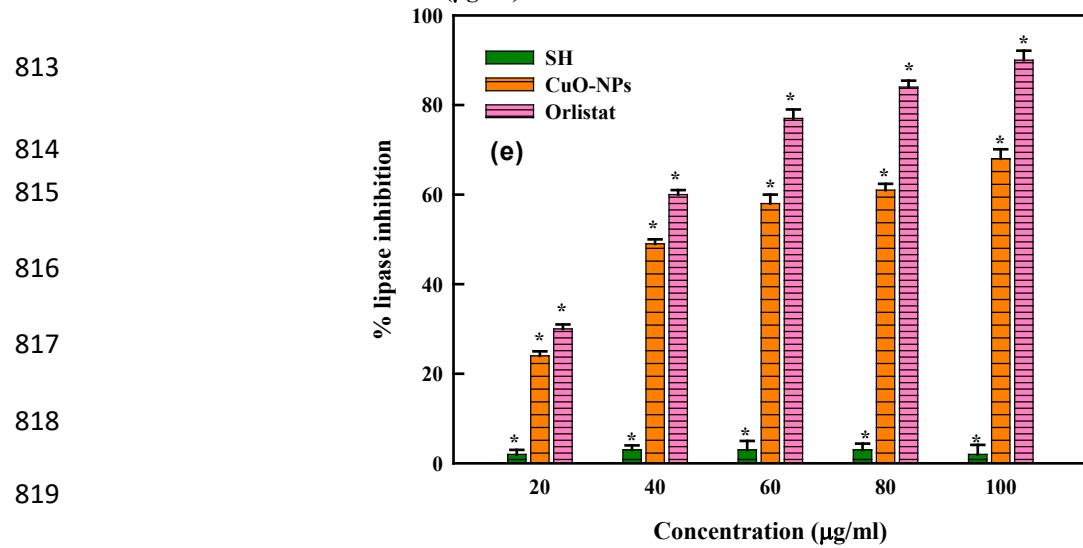
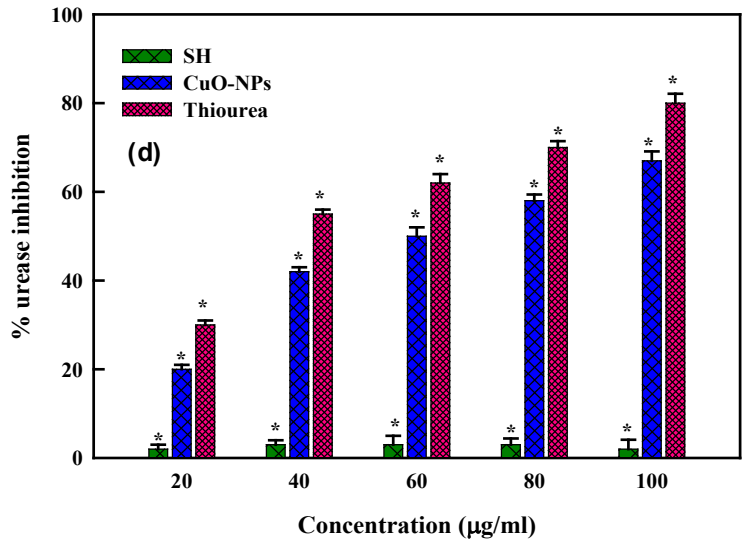
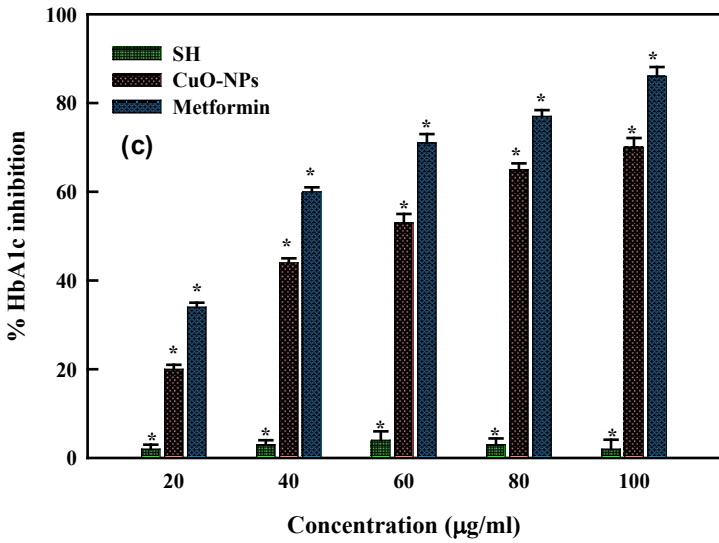
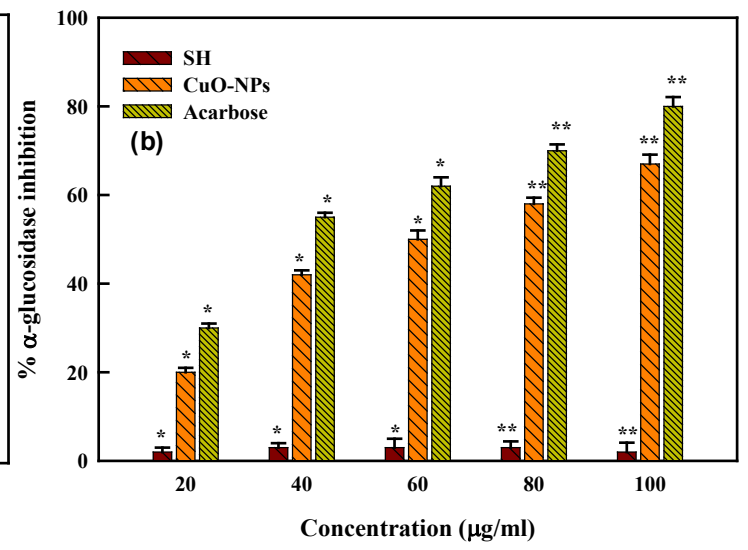
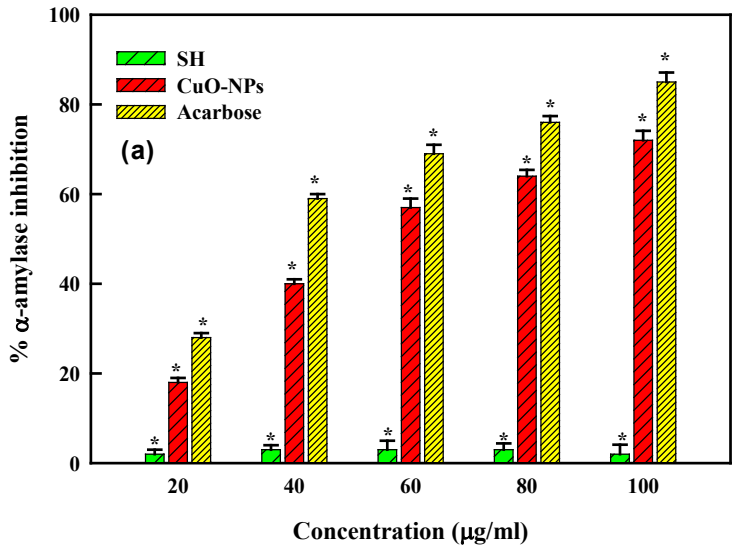
763 The H_2O_2 scavenging capacity of CuO-NPs was experimentally examined. Since,
764 the hydroxyl radical may harm a variety of molecules, including proteins, DNA, lipids,
765 and other highly reactive free radicals, it has been exploited as a highly destructive
766 species in free radical pathology [116, 117]. The findings of the current investigation
767 demonstrated that CuO-NPs had a greater potential for scavenging power with increase
768 in respective NPs concentrations (Fig. 7a). According to reports, CuO-NPs can produce
769 hydroxyl radicals when H_2O_2 is present. The capacity of CuO-NPs to scavenge free
770 radicals may be attributed to the presence of a number of biological constituents with
771 the ability to donate hydrogen atoms in their -OH groups. Also, the nitric oxide
772 scavenging activity of CuO-NPs increased with increasing concentrations of CuO-NPs
773 (Fig. 7b). From the aforementioned findings, it can be inferred that the biomolecules
774 adsorbed on CuO-NPs with antioxidant capacity may have contributed to the reduction
775 and stabilization of CuO-NPs during the synthetic process, hence increasing the
776 antioxidant activity of biosynthesized CuO-NPs. Similar results were also reported by
777 [1, 104, 118]. The reactive oxygen species can oxidize cell membranes, harm membrane
778 proteins, and alter DNA, which can lead to the beginning or worsening of a variety of
779 illnesses. Although, the body has a defense mechanism, ongoing contact with chemicals
780 and other contaminants can increase the amount of free radicals that the physiological
781 system of body cannot neutralize leading to irreparable oxidative damage [119-121]. In
782 order to prevent or treat oxidation-related disorders or free radicals, antioxidants with

783 the ability to neutralize free radicals are crucial. A focused strategy to the biochemical
784 preclusion of malignancies aimed at halt/return cellular system to their pre-cancerous
785 condition without the use of hazardous doses through foods and medications has to be
786 developed as a result of broad molecular cell level investigations on cancer cells [120,
787 122].

788 The peroxidase (POD) activity assay was used to analyze the capacity of SH-
789 assisted CuO-NPs in the degradation of hydrogen peroxide (H_2O_2). Both plants and
790 animals contain large amounts of enzyme peroxidases which catalyzes the oxidation of
791 several phenols and non-phenols derived substances by breaking down H_2O_2 . The
792 biosynthesized SH-CuO-NPs were found to be proficient biocatalysts exhibiting a
793 catalytic activity of 0.59 mM/min/mg in comparison to SH solution (0.05 mM/min/mg)
794 (Fig. 7c). Our findings were consistent with the earlier research, which reported that
795 CuO-NPs have peroxidase-like catalytic activity by the production of a blue-colored
796 product post nanoparticles addition to the TMB containing medium as a peroxidase
797 substrate [44, 100]. So, SH-assisted CuO-NPs are an excellent choice as peroxidase
798 mimics for a variety of possible applications due to their catalytic properties. The
799 metabolic process in mitochondria produces ROS and RNS as a byproduct. The DHR
800 123 probe was used to assess the amount of ROS/RNS. According to the findings shown
801 in Fig. 7d, the CuO-NPs generated more ROS and RNS in yeast cells than the control.
802 The CuO-NPs were found to generate up to 3400 ROS/RNS when incubated with yeast
803 cells, compared with control (610 ROS/RNS). In general, mitochondrial respiration
804 produces free radicals, with electron transport chain (ETC) serving as the site of ROS
805 production and oxygen leakage. The relevance of metallic nanoparticles improved the
806 ability of fenton reaction in the production of free radicals. Additionally, the metallic
807 ions in nanoparticles can prevent mitochondrial electron transport, increasing the

808 formation of ROS. Similar outcomes were noted in earlier studies where the use of
809 metal derived nanoparticles led to ROS generation [123]. The cellular mechanism was
810 severely compromised due to the increased levels of ROS/RNS caused by an imbalance
811 between the free radicals and their scavenging activity.

812

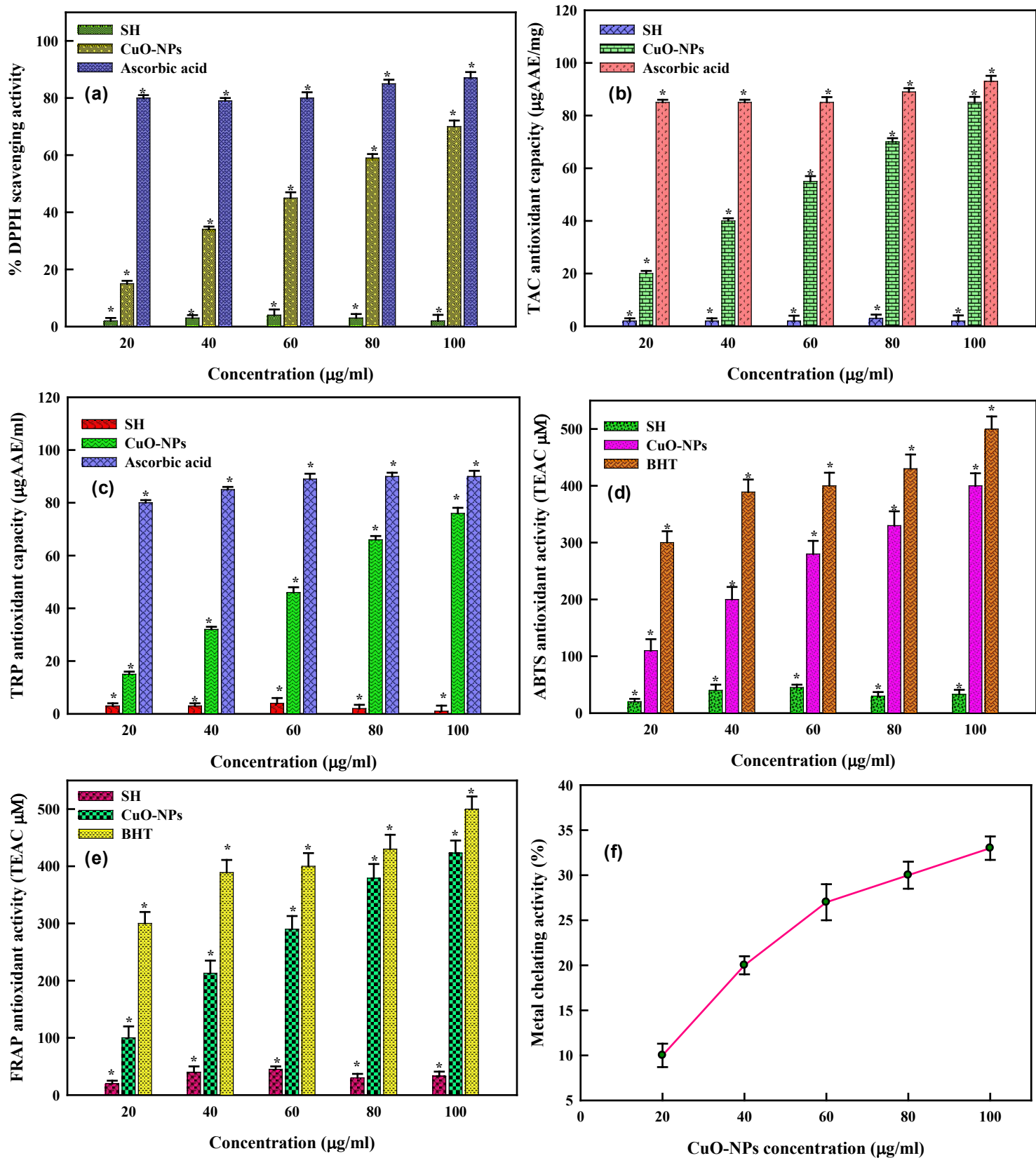


813
814
815
816
817
818
819

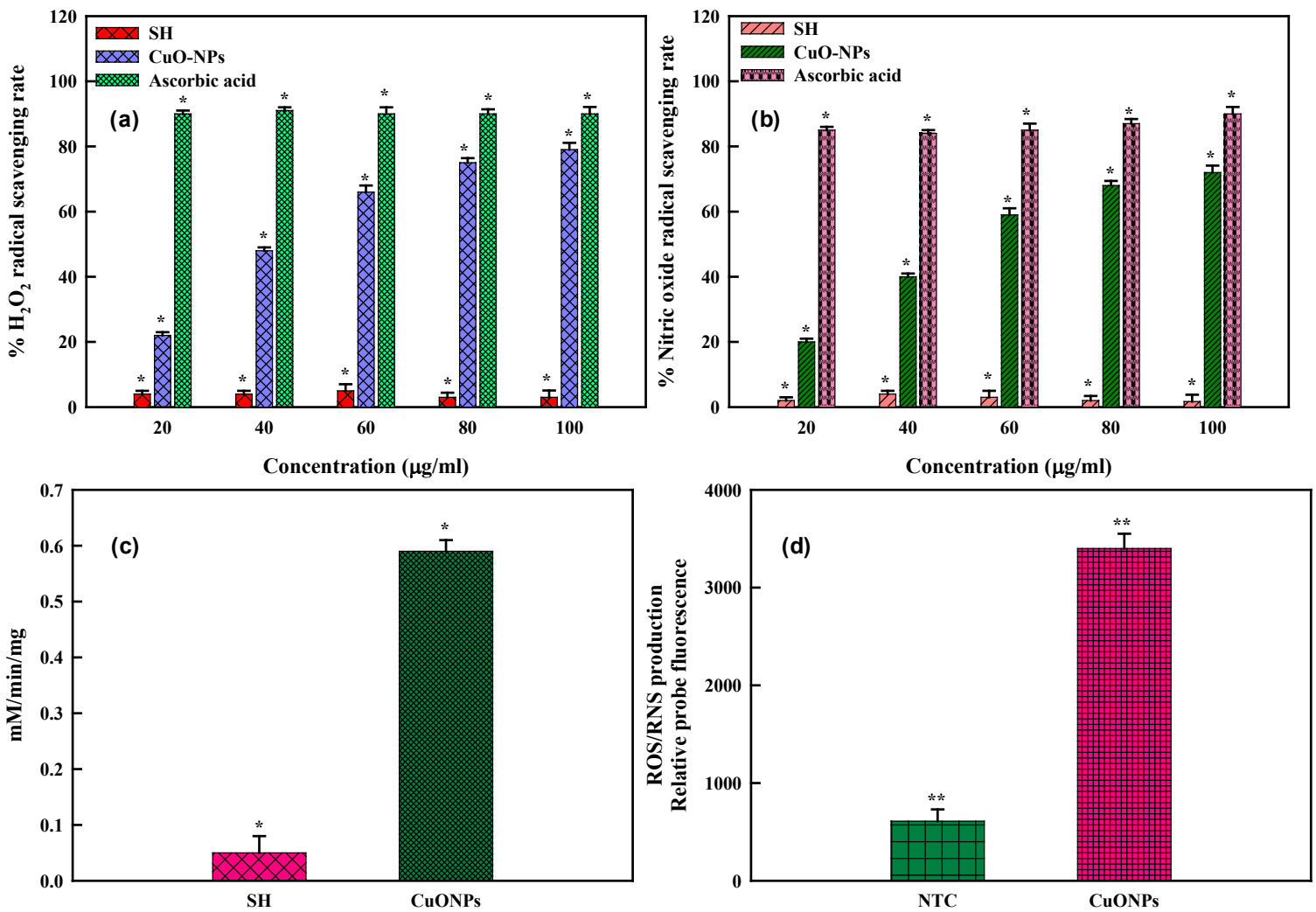
820

821

822 **Fig. 5** Biological activity of CuO-NPs. (a) α -amylase, (b) α -glucosidase, (c) HbA1c,(d) urease and
823 (e) lipase inhibitory activities.



824 **Fig. 6** Antioxidant activity of CuO-NPs. (a) DPPH, (b) TAC, (c) TRP, (d) ABTS, (e) FRAP and (f)
 825 metal chelation activities.



826 **Fig. 7** Antioxidant activities of CuO-NPs. (a) H₂O₂ radical scavenging activity, (b) NO₂ radical
 827 scavenging activity, (c) peroxidase-like catalytic activity, (d) ROS/RNS measurement (NTC=non
 828 treated cells).

829 Antibiotic resistance is one of the most serious public health problems, which is
 830 caused by inappropriate or excessive use of antibiotics [1, 3, 124, 125]. The urgent need
 831 to develop new antibiotic agents, use active and widespread techniques of infection
 832 control to stop the development of antibiotic resistant strains, and prolong treatment
 833 including hospitalization and recovery all contribute to increased healthcare costs. The
 834 occurrence of fatal and hazardous adverse effects from utilizing antibiotics in treatment,

835 such as anaphylactic shock (or hypersensitivity reactions), growth suppression of
836 hematopoietic stem cells, and liver and kidney failure in some patients, are the
837 additional issues. Even while only a small number of patients may experience these
838 consequences, they are nonetheless significant because they can be fatal and harmful.
839 The use of nanoparticles in medicine and related fields has grown significantly as a
840 result of the development of nanotechnology science and the discovery of their
841 antibacterial characteristics [126]. Also, the resistance of many infections to antibiotics is
842 one of the primary issues facing medical science, the potential antibacterial actions of
843 biosynthesized nanoparticles are crucial. In current study, the agar well diffusion
844 technique was used to assess the antibacterial efficacy of green produced SH-assisted
845 CuO-NPs against both gram +ve and gram-ve pathogenic bacteria (Fig. 8a). The tested
846 bacterial strains were effectively inhibited by CuO-NPs with the maximal zone of
847 inhibition reported in *E. coli* (27 mm) followed by *S. aureus* (22 mm). No inhibition was
848 reported in negative control setup. Also, the cellular leakage of biological molecules like
849 proteins and nucleic acids increased with successive increase in CuO-NPs
850 concentrations (Fig. 8b and c). The *E. coli* cells exhibited higher levels of protein leakage
851 (112 µg/ml) than *S. aureus* (78 µg/ml) post 6h time treatment. Similar results were also
852 observed in nucleic acid leakage in which *E. coli* cells (0.2 OD₂₆₀) leaked more amounts of
853 nucleic acids than *S. aureus* (0.11 OD₂₆₀) post 6h treatment. Both intracellular and
854 extracellular interactions may be responsible for the antibacterial activity of CuO-NPs
855 against human pathogenic organisms [127, 128]. The potential interaction between the
856 CuO-NPs and the outer bacterial membrane may be due to growth suppression by the
857 former. CuO-NPs have the potential to compromise bacterial cell viability by impairing
858 enzyme performance and increasing cell permeability [129, 130]. CuO-NPs may also
859 integrate within cell membrane owing to their small size compared to the membranal

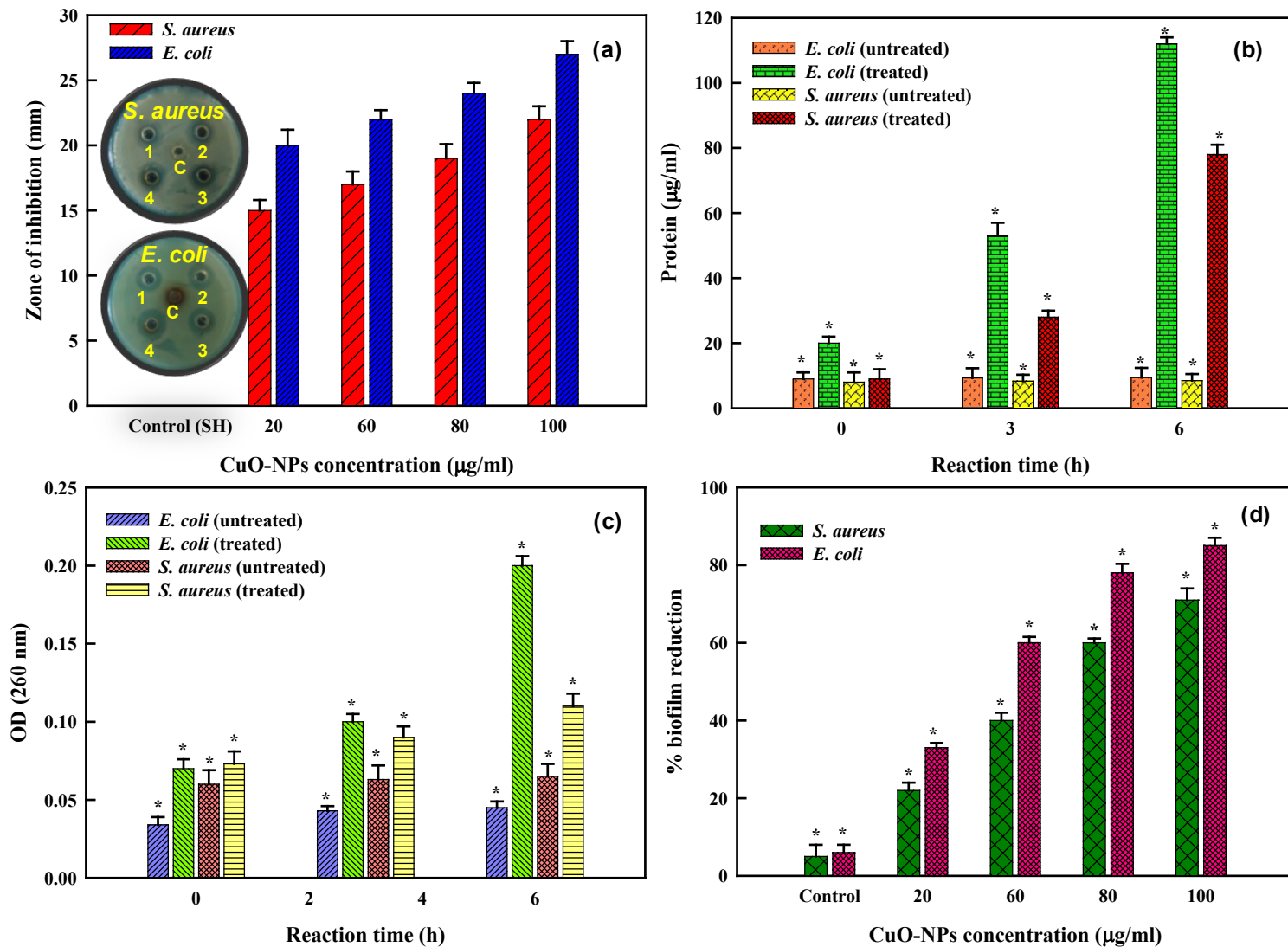
860 pores on bacterial cell surface. Additionally, CuO-NPs produce reactive oxygen species
861 like hydroxyl and superoxide free radicals, which harm cells by oxidizing double
862 bonding of phospholipids and disrupting membrane permeability, leading to high
863 osmotic stress and finally leading to bacterial cell death [131, 132] (Fig. 9).

864 An urgent necessity exists to investigate novel approaches to treat infections and
865 diseases linked to bacterial biofilm as a result of the emergence of MDRB (multi drug
866 resistant bacteria) based biofilm-associated infections. The contents of bacterial biofilm
867 based on constitutive components are broadly classified into: hydrophobic
868 (lipopolysaccharides, lipids, surfactants) and hydrophilic (proteins, nucleic acids,
869 polysaccharides) [133]. The anti-biofilm action of nanoparticles (NPs) is significantly
870 influenced by a number of factors, like charge, size distribution, hydrophobicity, surface
871 chemistry, etc. The NPs interact and penetrate biofilm compartments when positioned
872 adjacent to the biofilm [134]. In this study, the biofilm inhibitory potential of CuO-NPs
873 against the cells of *E. coli* and *S. aureus* was evaluated. The CuO-NPs concentrations (20-
874 100 µg/ml) inhibited the formation of biofilm compared to control (Fig. 8d). The CuO-
875 NPs concentrations of 20, 60, 80 and 100µg/ml decreased the biofilm formation (in *E. coli*
876 cells) by 33.1%, 60.02%, 78.4%, 85.32% and (in *S. aureus* cells) by 22.3%, 40.12%, 60.34%,
877 71.2%, respectively. In agreement with our outcomes, Oliver *et al.* [135] reported 99.9%
878 biofilm reduction at 5 µg/ml AgNPs while no discernible anti-biofilm effect was
879 exhibited by citrate-reduced AgNPs. Strains of *S. aureus* and other biofilm forming
880 bacteria are the principal microbial species responsible for the nosocomial infections
881 linked to catheters. It is demonstrated that catheters coated with metallic nanoparticles
882 significantly inhibit the in-vitro biofilm producing ability of pathogens. Additionally,
883 the consistent release of metallic ions was helpful for patients with invasive devices.

884 The metallic nanoparticles might stop the respiratory enzymes and electron
885 transporters of the pathogens, leading to bacterial death [1].

886 DNA typically interacts with metal complexes in a variety of ways, and these
887 interactions have a significant impact on the structure and function of DNA [136]. They
888 have a strong affinity for DNA and have the ability to cause DNA cleavage [136]. The
889 bio-efficacy of majority of the anticancer medications is frequently correlated with their
890 DNA interaction capacity. Such substances can cause apoptosis and inhibit cell
891 proliferation in cancer cells by destroying their DNA structure [136]. Hence, the ability
892 of SH-assisted CuO-NPs to cleave DNA was evaluated using agarose gel
893 electrophoresis. It is an effective method for identifying DNA damage. DNA is broken
894 at specified sequence areas on the genome during agarose electrophoresis for DNA
895 typing [137]. The transformation of pBR322 DNA form from supercoiled circular
896 conformation (Form I) to nicked circular conformation (Form II) and linear
897 conformation (Form III) serves as a DNA cleavage check. The nuclease activity was
898 visible in all concentrations of CuO-NPs (Fig. 10). Control experiments using pBR322
899 plasmid DNA didn't show any DNA cleavage activity (Lane 1). At 20 $\mu\text{g/ml}$, the
900 supercoiled plasmid DNA was transformed into circular shape. However, at greater
901 concentrations (60 and 100 $\mu\text{g/ml}$), Form I was transformed into more dense Form III.
902 Based on the results, SH-assisted CuO-NPs served as a powerful chemical nuclease for
903 the breaking of double strand DNA; demonstrating their potential as a DNA target
904 agent and an alternative cancer treatment. Similar reports were reported by the studies
905 of [1, 136-138].

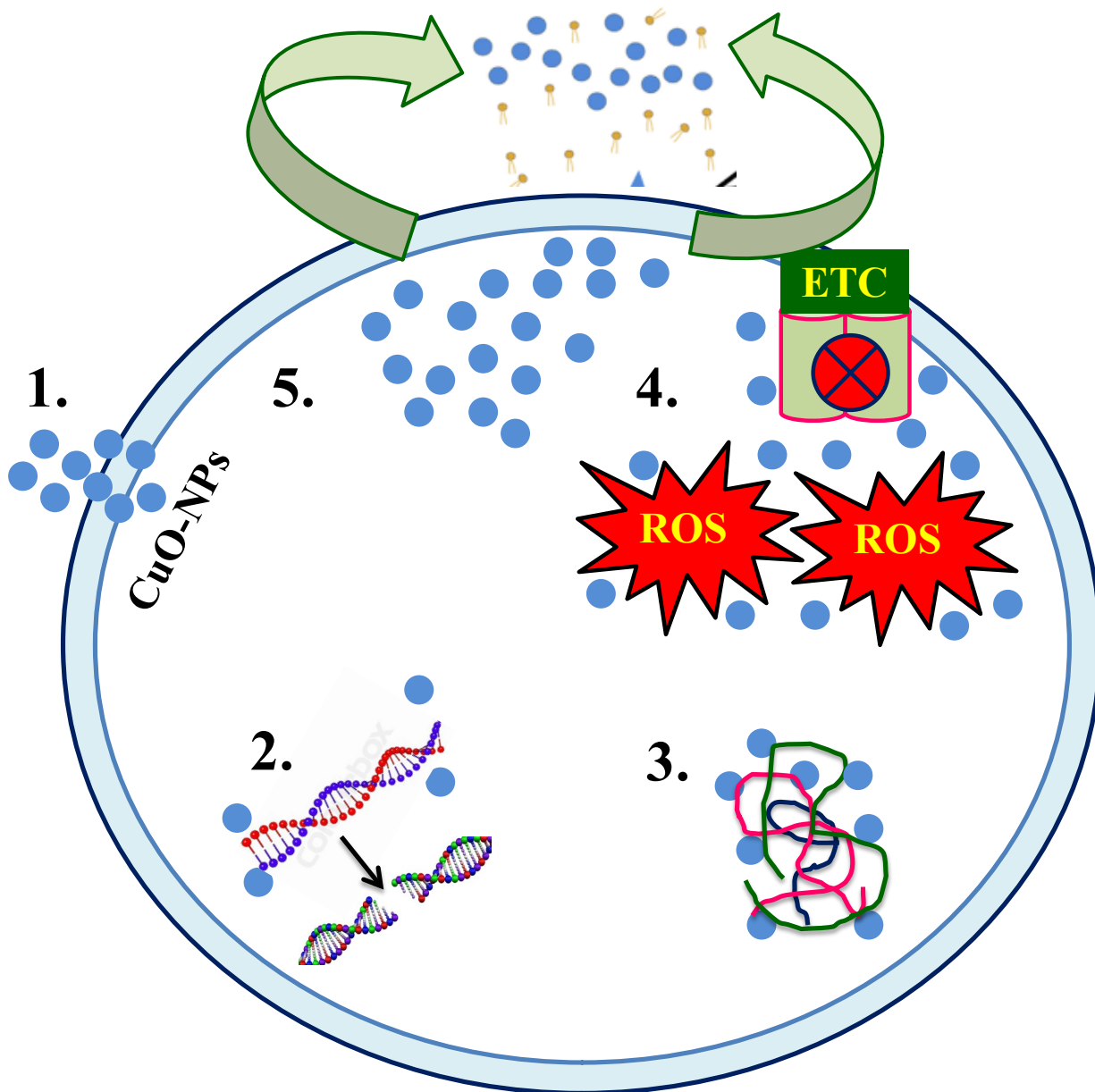
906
907



908 **Fig. 8** Antibacterial activity of CuO-NPs (a) well diffusion assay, (b) protein leakage, (c) nucleic
 909 acid leakage, and (d) antibiofilm activity.

910

911



913

914

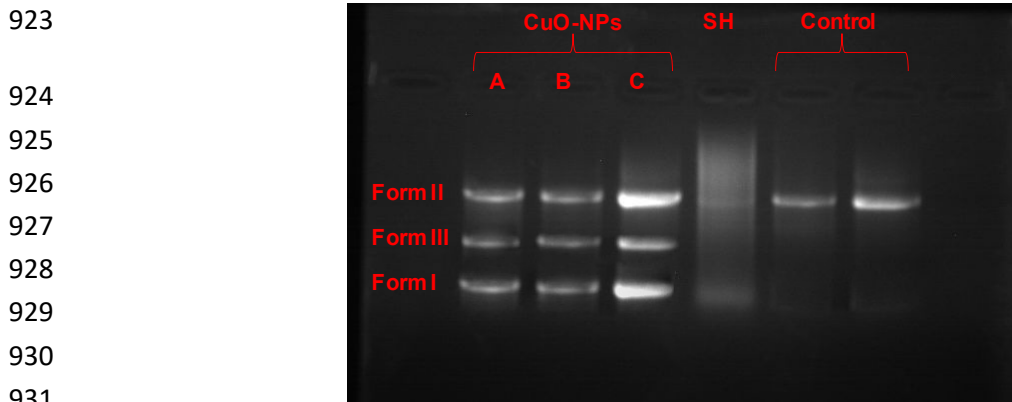
915 **Fig. 9** Mechanism of antibacterial activity of CuO-NPs.916 1. Interaction of CuO-NPs with cellular membrane; leading to decreased transmembrane
917 electrochemical potential affecting membrane integrity.

918 2. DNA damage due to interaction with CuO-NPs.

919 3. Interaction of Cu²⁺ ions with sulfhydryl groups of proteins.

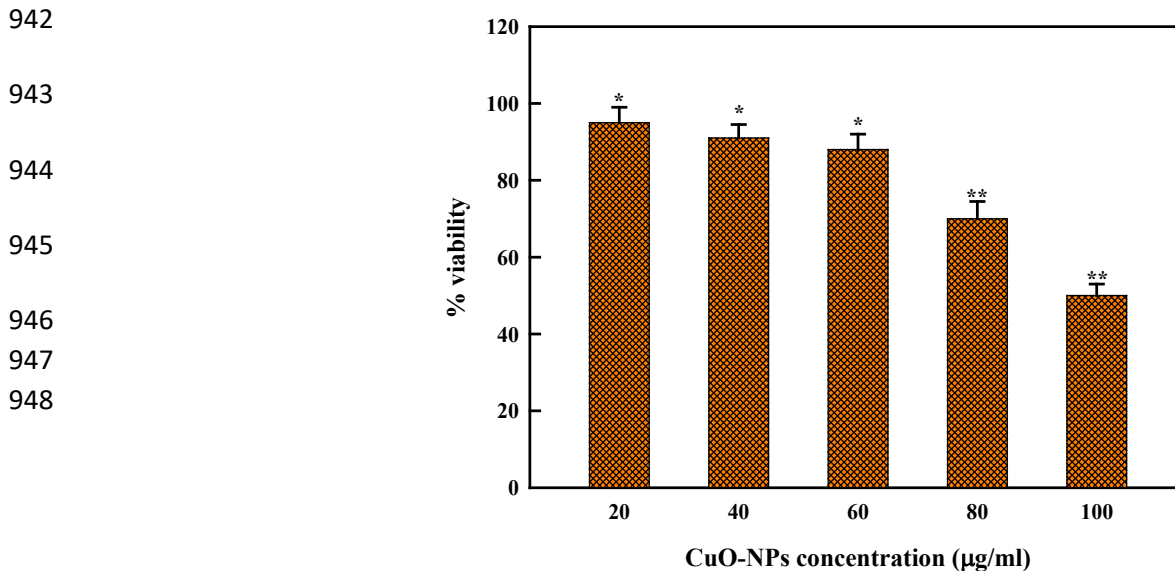
920 4. Entry of CuO-NPs and Cu²⁺ ions inside cell; creating oxidative stress which leads to cell
921 death.

922 5. Accumulation of CuO-NPs on cell surface leaking to cell leakage.



932 **Fig. 10** Cleavage patterns with various concentrations of CuO-NPs.(A) 20 µg/ml, (B) 60 µg/ml,
933 (C) 100 µg/ml, Control= pBR622.

934 The brine shrimp (*Artemia*) is a common model organism used in the
935 toxicological experiments and is a useful substitute in assessing the effects of marine
936 toxicity. In present work, the cytotoxicity of CuO-NPs was investigated on brine shrimp
937 nauplii at different concentrations (20-100 µg/ml) (Fig. 11). The results exhibited that the
938 viability of nauplii decreased in a concentration-dependent pattern; from 95% (20
939 µg/ml) to 50% (100 µg/ml) which can be ascribed to the effects exerted by the higher
940 concentrations of CuO-NPs. The effects of CuO-NPs were found to be statistically
941 significant ($p < 0.001$). Similar results were also reported by the studies of [139-140]

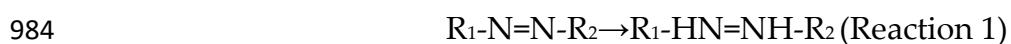


949
950
951

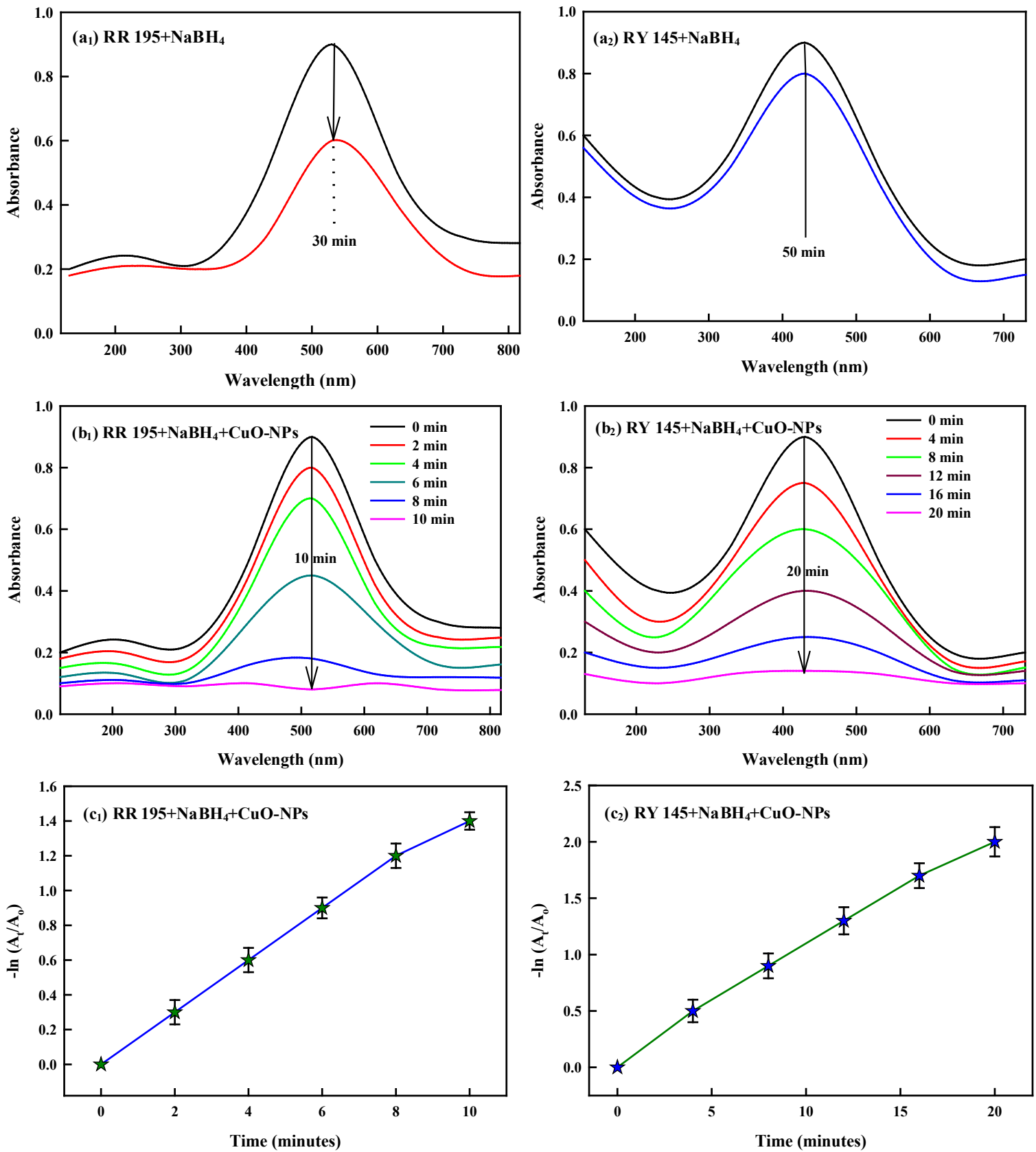
Fig. 11 Cytotoxicity of CuO-NPs against brine shrimp

952 The primary organic contaminants in wastewater, azo dyes are thought to be
953 extremely hazardous, mutagenic, carcinogenic, teratogenic [95, 141-143]. In this study,
954 dyes RR195 and RY145 were used as a model azo dye compounds to examine the
955 catalytic effectiveness of SH assisted CuO-NPs as a nanocatalyst in the presence of
956 NaBH₄ well elucidated by time-dependent absorption curves (Fig.12). Firstly, the
957 absorption peaks of dyes RR195 and RY145 were documented at 530 nm and 430 nm,
958 respectively. The degradation experiment was conducted after recording their
959 intensities as a function of time. The addition of CuO-NPs alone noted a small decrease
960 in the intensities of dyes RR195 and RY145 (data not shown). Also, there was only a
961 7.94% and 13.22% fall in RR195 and RY145 by 50 minutes under NaBH₄ alone in the
962 breakdown of azo dyes, indicating an incomplete dye breakdown (Fig.12: a1–a2)
963 attributable to simple surface absorption (Reaction 1), instead of dye breakdown.
964 However, when NaBH₄ coupled CuO-NPs were added to the dye solution, there was a
965 significant drop in the intensity of the absorption (Fig.12: b1–b2). As the reaction
966 proceeded, the dye hue disappeared turning the reaction mixture to clear solution,
967 indicating the breakdown of dyes. The rate of degradation of dyes RR195 and RY145
968 were found to be 93% and 91%, respectively. However, the appearance of lower band
969 peak following the reduction process shows that the azo dye decolorization was
970 achieved by the breakdown of azo structure as opposed to merely physical adsorption,
971 indicating the conversion of azo dyes into the equivalent amine compounds (Reaction
972 2). Since the dye concentration at a given time (C_t) was directly proportional to the
973 absorbance values at that time (A_t), the reaction followed pseudo-first-order kinetics.
974 From the linearity of $\ln(A_t/A_0)$ vs t plot, the kinetic rate constants (k) of RR195 and

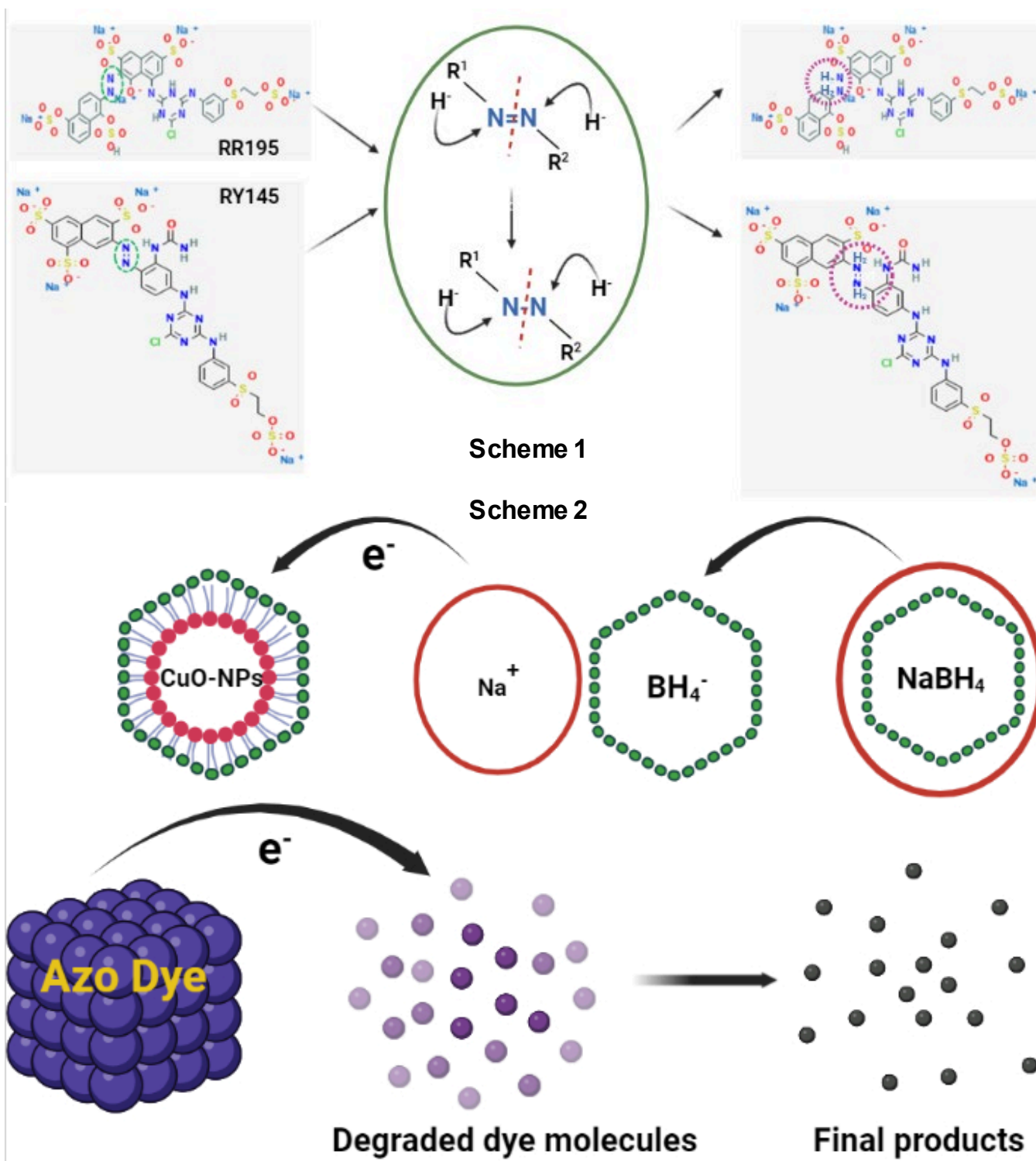
975 RY145 was found to be as 0.0941 and 0.0220 min⁻¹, respectively calculated straight for
976 the straight-line slope (Fig.12: c1–c2). It is important to note that dye RR195 degraded
977 relatively faster than dye RY145 which may possibly be due to the steric barrier of
978 additional groups close to -N=N- in the latter molecule. The three steps can be used to
979 describe the reduction mechanism: (i) Adsorption of azo elements and BH₄⁻ by CuO-
980 NPs, (ii) the transfer of electron (e⁻) from BH₄⁻ to dye molecules via CuO-NPs, (iii) the
981 reaction of Cu²⁺ with dye molecules and (iv) the conversion of colorful dye (-N=N-) into
982 monochrome amines (-NH₂ + H₂N-) compounds. Similar mechanism of dye
983 degradation was also reported by [16, 17, 144].



986 As a result, Scheme 1 updates the reaction mechanism with precise
987 specifications. Here, SH serves as a stabilizer to prevent any aggregation and maintain
988 the catalytic activity of the biosynthesized nanoparticle. The dye elements are adsorbed
989 on the exterior of CuO-NPs due to the presence of biopolymer clad nanoparticles,
990 without affecting their function [145]. Additionally, as the reducing agents such as
991 NaBH₄ were introduced into the reaction system, the nanoparticles instantly absorbed
992 them, reducing the reductive strength significantly. However, the capping of SH on the
993 nanoparticle validated the regular electron flow from nucleophilic NaBH₄ to dye
994 oxidation [145]. As a result, the azo dyes were easily absorbed by electrons, causing a
995 redox reaction that destroyed dye chromophore structure and led to the production of
996 amine species [146]. Schematically, Scheme 2 illustrates the advantage of biopolymer
997 with respect to dye degradation using SH-assisted CuO-NPs via electron transfer from
998 NaBH₄ nucleophile.



999 **Fig. 12** Absorption with (a₂–b₂) and without (a₁–b₁) CuO-NPs, and linear relationship of
 1000 $\ln(A_t/A_0)$ (c₁–c₂) for the catalytic dye reduction.



1001
 1002 **Scheme 1** Using a biocatalyst with a NaBH₄ coupling, RR195 and RY145 are effectively
 1003 degraded.

1004 **Scheme 2** provides an illustration of the process involved in the use of CuO-NPs by NaBH₄
1005 nucleophile to move electrons in favour of biopolymer in dye decomposition.

1006

1007 4. Conclusion

1008 In conclusion, SH-assisted CuO-NPs were formed, for the first time, in an
1009 environmentally friendly, one-pot method in which SH macromolecules served as
1010 stabilizing and reducing agents for CuO-NPs in the SH-matrix. Without employing any
1011 harmful reagents, the reaction parameters were standardized to maximize the yield of
1012 CuO-NPs. The CuO-NPs fabricated using the sustainable chemistry approach were
1013 extremely crystalline, well-capped and well-dispersed CuO-NPs by SH-macromolecules
1014 and have a spherical/oval shape measuring 17.4 ± 1.3 nm with an elemental composition
1015 of 29.49%. The FT-IR spectra exhibited the presence of many carboxyl and hydroxyl
1016 groups which helped in the maintenance of monodispersed state by electrostatic
1017 repulsion. The biosynthesized CuO-NPs exhibited notable bactericidal (*E. coli*
1018 {inhibition zone 27mm; biofilm inhibition 85.32%; *S. aureus* [inhibition zone 22mm;
1019 biofilm inhibition 71.2%]) and antioxidant [FRSA ($70 \pm 2.3\%$), TAC ($85 \pm 0.26\%$), TRP
1020 ($76 \pm 0.35\%$), ABTS (400 μ m TEAC), FRAP (423 μ m TEAC)] activities. The increased
1021 activities of enzymes like urease ($68 \pm 2.1\%$), lipase ($70 \pm 2.3\%$), peroxidase (0.59
1022 mM/min/mg), ROS/RNS 3400 counts of relative probe fluorescence, metal chelation
1023 (33%) and cell leakage assays of protein (*E. coli* 112 μ g/ml; *S. aureus* 78 μ g/ml) and
1024 nucleic acids (*E. coli* OD 0.2; *S. aureus* OD 0.11) were reported in the presence of CuO-
1025 NPs. Furthermore, the CuO-NPs exhibited enhanced anti-diabetic activity against
1026 enzymes α -amylase ($72 \pm 1.2\%$) and α -glucosidase ($70 \pm 2.1\%$). Also, the combination of
1027 intrinsic time-dependent absorptive spectra and mechanics of pseudo-first-order
1028 reaction kinetics demonstrated biosynthesized CuO-NPs as efficient nanocatalysts for
1029 azo dyes decomposition (91-93% rate of degradation) and hold great promise in the
1030 fields of industrial wastewater treatment.

1031 **Author contributions**

1032 Conceptualization, T.C.; formal analysis, T.C.; investigation, T.C.; methodology,
1033 T.C., data curation, T.C., C.R.; validation, T.C., W.J.; writing—original draft, T.C.;
1034 writing—review and editing, I.N; writing—review and editing, T.C., C.R., R.K.V.R, J.J.,
1035 W.J., C.K. All authors have read and agreed to the published version of the manuscript.

1036 **Acknowledgments**

1037 The first author is sincerely grateful to Mar Athanasios College for Advanced
1038 Studies Tiruvalla (MACFAST) for offering facilities for laboratories and infrastructural
1039 support.

1040 **Conflicts of Interest**

1041 The authors declare no conflict of interest.

1042 **References**

- 1043 [1] T. Cherian, D. Maity, R.T. Rajendra Kumar, G. Balasubramani, C. Ragavendran,
1044 S. Yalla, R. Mohanraju, W.J.G.M. Peijnenburg, Green chemistry based gold
1045 nanoparticles synthesis using the marine bacterium *Lysinibacillus odyseeyi* PBCW2
1046 and their multitudinous activities, *Nanomater.* 12 (2022) 2940.
- 1047 [2] T. Cherian, K. Ali, S. Fatima, Q. Saquib, S.M. Ansari, H.A. Alwathnani, A.A. Al-
1048 Khedhairi, M. Al-Shaeri, J. Musarrat, *Myristica fragrans* bio-active ester
1049 functionalized ZnO nanoparticles exhibit antibacterial and antibiofilm activities
1050 in clinical isolates, *J. Microbiol. Methods.* 166 (2019) 105716.
- 1051 [3] T. Cherian, K. Ali, Q. Saquib, M. Faisal, R. Wahab, J. Musarrat, *Cymbopogon*
1052 *citratus* functionalized green synthesis of CuO nanoparticles: Novel prospects as
1053 antibacterial and antibiofilm agents, *Biomol.* 10 (2020) 169.
- 1054 [4] A. Verma, S.P. Gautam, K.K. Bansal, N. Prabhakar and J.M. Rosenholm, *Green*
1055 *Nanotechnology: Advancement in phytoformulation research, Medicines* 6 (1)
1056 (2019) 39; <https://doi.org/10.3390/medicines6010039>.
- 1057 [5] S. Ghotekar, S. Pansambal, M. Bilal, S.S. Pingale, R. Oza, Environmentally
1058 friendly synthesis of Cr₂O₃ nanoparticles: Characterization, applications and
1059 future perspective- a review, *Case Studies in Chemical and Environmental*
1060 *Engineering* 3 (2021) 100089.

- 1061 [6] T. Pagar, S. Ghotekar, S. Pansambal, R. Oza, B.P. Marasini, Facile plant extract
1062 mediated eco-benevolent synthesis and recent applications of CaO-NPs: a state-
1063 of the- art review, *J. Chem. Rev.* 2 (3) (2020) 201–210,
1064 <https://doi.org/10.22034/JCR.2020.107355>.
- 1065 [7] X. Zhang, C. Huang, S. Mahmud, X. Guo, X. Hu, Y. Jing, S. Su, J. Zhu, Sodium
1066 alginate fasten cellulose nanocrystal Ag@AgCl ternary nanocomposites for the
1067 synthesis of antibacterial hydrogels, *Compos. Commun.* 25 (2021) 100717.
- 1068 [8] A. Naghizadeh, Z.M. Mizwari, S.M. Ghoreishi, S. Lashgari, S. Mortazavi-
1069 Derazkola, B. Rezaie, Biogenic and eco-benign synthesis of silver nanoparticles
1070 using jujube core extract and its performance in catalytic and pharmaceutical
1071 applications: Removal of industrial contaminants and in-vitro antibacterial and
1072 anticancer activities, *Environ. Technol. Innov.* 23 (2021) 101560.
- 1073 [9] M. Shirzadi-Ahodashti, Z.M. Mizwari, Z. Hashemi, S. Rajabalipour, S.M.
1074 Ghoreishi, S. Mortazavi-Derazkola, M.A. Ebrahimzadeh, Discovery of high
1075 antibacterial and catalytic activities of biosynthesized silver nanoparticles using
1076 *C. fruticosus* (CF-AgNPs) against multi-drug resistant clinical strains and
1077 hazardous pollutants, *Environ. Technol. Innov.* 23 (2021) 101607.
- 1078 [10] S.A. Akintelu, S.C. Olugbeko, A.S. Folorunso, A review on synthesis,
1079 optimization, characterization and antibacterial application of gold nanoparticles
1080 synthesized from plants, *Int. Nano Lett.* (2020) 1–12.
- 1081 [11] F. Abdelghaffar, Biosorption of anionic dye using nanocomposite derived
1082 from chitosan and silver nanoparticles synthesized via cellulosic banana peel bio-
1083 waste, *Environ. Technol. Innov.* 24 (2021) 101852.
- 1084 [12] K.C. Majhi, M. Yadav, Chapter 5 - synthesis of inorganic nanomaterials
1085 using carbohydrates. In: Inamuddin Boddula, R., Ahamed, M.I., Asiri, A.M.
1086 (Eds.), *Green Sustainable Process for Chemical and Environmental Engineering*
1087 *and Science*. Elsevier (2021) pp. 109–135.
- 1088 [13] K.M.F. Hasan, H. Wang, S. Mahmud, C. Genyang, Coloration of aramid
1089 fabric via in-situ biosynthesis of silver nanoparticles with enhanced antibacterial
1090 effect, *Inorg. Chem. Commun.* 119 (2020a) 108115.
- 1091 [14] K.M.F. Hasan, H. Wang, S. Mahmud, M.A. Jahid, M. Islam, W. Jin, C.
1092 Genyang, Colorful and antibacterial nylon fabric via in-situ biosynthesis of
1093 chitosan mediated nanosilver, *J. Mater. Res. Technol.* 9 (6) (2020b) 16135–16145.
- 1094 [15] Y. Xiong, L. Huang, S. Mahmud, F. Yang, H. Liu, Bio-synthesized
1095 palladium nanoparticles using alginate for catalytic degradation of azo-dyes,
1096 *Chin. J. Chem. Eng.* 28 (5) (2020) 1334–1343.

- 1097 [16] H. Wan, C. Li, S. Mahmud, H. Liu, Kappa carrageenan reduced-stabilized
1098 colloidal silver nanoparticles for the degradation of toxic azo compounds,
1099 *Colloids Surf. A* 616 (2021a) 126325.
- 1100 [17] H. Wan, Z. Liu, Q. He, D. Wei, S. Mahmud, H. Liu, Bioreduction (Au^{III} to
1101 Au⁰) and stabilization of gold nanocatalyst using Kappa carrageenan for
1102 degradation of azo dyes, *Int. J. Biol. Macromol.* 176 (2021b) 282–290.
- 1103 [18] S. Mahmud, N. Pervez, M.A. Taher, K. Mohiuddin, H.-H. Liu,
1104 Multifunctional organic cotton fabric based on silver nanoparticles green
1105 synthesized from sodium alginate, *Textile Res. J.* 90 (11–12) (2020) 1224–1236.
- 1106 [19] J. Chen, Y. Liu, Y. Xiong, D. Wei, J. Peng, S. Mahmud, H. Liu, Konjac
1107 glucomannan reduced-stabilized silver nanoparticles for mono-azo and di-azo
1108 contained wastewater treatment, *Inorg. Chim. Acta* 515 (2021a) 120058.
- 1109 [20] J. Chen, D. Wei, L. Liu, J. Nai, Y. Liu, Y. Xiong, J. Peng, S. Mahmud, H.
1110 Liu, Green synthesis of konjac glucomannan templated palladium nanoparticles
1111 for catalytic reduction of azo compounds and hexavalent chromium, *Mater.*
1112 *Chem. Phys.* 267 (2021b) 124651.
- 1113 [21] Y. Xiong, H. Wan, M. Islam, W. Wang, L. Xie, S. Lü, S.M. Fijul Kabir, H.
1114 Liu, S. Mahmud, Hyaluronate macromolecules assist bioreduction (Au^{III} to Au⁰)
1115 and stabilization of catalytically active gold nanoparticles for azo contaminated
1116 wastewater treatment, *Environ. Technol. Innov.* 24 (2021) 102053.
- 1117 [22] J. Sequeira, B.S. Rao, P.R. Kedia, Efficacy of sodium hyaluronate for
1118 temporomandibular joint disorder by single-puncture arthrocentesis, *J.*
1119 *Maxillofacial Oral Surg.* 18 (1) (2019) 88.
- 1120 [23] M.H. El-Dakdouki, D.C. Zhu, K. El-Boubbou, M. Kamat, J. Chen, W. Li, X.
1121 Huang, Development of multifunctional hyaluronan-coated nanoparticles for
1122 imaging and drug delivery to cancer cells, *Biomacromol.* 13 (4) (2012) 1144–1151.
- 1123 [24] F. Namvar, S. Azizi, H.S. Rahman, R. Mohamad, A. Rasedee, M. Soltani,
1124 R.A. Rahim, Green synthesis, characterization, and anticancer activity of
1125 hyaluronan/zinc oxide nanocomposite, *OncoTargets Therapy.* 9 (2016) 4549.
- 1126 [25] K.M. Rao, M. Suneetha, S. Zo, K.H. Duck, S.S. Han, One-pot synthesis of
1127 ZnO nanobelt-like structures in hyaluronan hydrogels for wound dressing
1128 applications, *Carbohydr. Polymers.* 223 (2019) 115124.
- 1129 [26] G. Khachatryan, K. Khachatryan, J. Grzyb, M. Fiedorowicz, Formation and
1130 properties of hyaluronan/nano Ag and hyaluronan-lecithin/nano Ag films,
1131 *Carbohydr. Polymers.* 151 (2016) 452–457.
- 1132 [27] N. Xia, Y. Cai, T. Jiang, J. Yao, Green synthesis of silver nanoparticles by
1133 chemical reduction with hyaluronan, *Carbohydr. Polymers.* 86 (2) (2011) 956–961.

- 1134 [28] R. Abdel-Mohsen, L. Hrdina, G. Burgert, R.M. Krylová, A. Abdel-Rahman,
1135 M. Krejčová, L. Beneš Steinhart, Green synthesis of hyaluronan fibers with silver
1136 nanoparticles, *Carbohydr. Polymers* 89 (2) (2012) 411–422.
- 1137 [29] J.-P. Deng, S.-H. Li, S.-T. Chang, Y.-C. Shih, Hyaluronan-assisted synthesis
1138 of silver nanoparticles and nanowires, *Res. Chem. Intermed.* 45 (1) (2019) 119–
1139 125.
- 1140 [30] X. Zhang, M. Yao, M. Chen, L. Li, C. Dong, Y. Hou, H. Zhao, B. Jia, F.
1141 Wang, Hyaluronic acid-coated silver nanoparticles as a nanoplatform for in vivo
1142 imaging applications, *ACS Appl. Mater. Interfaces*. 8 (39) (2016) 25650–25653.
- 1143 [31] H.-J. Li, A.-Q. Zhang, L. Sui, D.-J. Qian, M. Chen, Hyaluronan/tween 80-
1144 assisted synthesis of silver nanoparticles for biological application, *J.*
1145 *Nanoparticle Res.* 17 (2) (2015) 1–13.
- 1146 [32] N.Q. Hien, D. Van Phu, N.N. Duy, Radiation synthesis and
1147 characterization of hyaluronan capped gold nanoparticles, *Carbohydr. Polymers.*
1148 89 (2) (2012) 537–541.
- 1149 [33] H.S. Han, K.Y. Choi, H. Lee, M. Lee, J.Y. An, S. Shin, S. Kwon, D.S. Lee,
1150 J.H. Park, Gold-nanoclustered hyaluronan nano-assemblies for photothermally
1151 maneuvered photodynamic tumor ablation, *ACS Nano*. 10 (12) (2016) 10858–
1152 10868.
- 1153 [34] M.M. Kemp, A. Kumar, S. Mousa, T.-J. Park, P. Ajayan, N. Kubotera, S.A.
1154 Mousa, R.J. Linhardt, Synthesis of gold and silver nanoparticles stabilized with
1155 glycosaminoglycans having distinctive biological activities, *Biomacromolecul.* 10
1156 (3) (2009) 589–595.
- 1157 [35] N. Verma and N. Kumar, Synthesis and biomedical applications of copper
1158 oxide nanoparticles: an expanding horizon, *ACS Biomater. Sci. Eng.* 5 (2019)
1159 1170–1188.
- 1160 [36] W. M. Rangel, R.A.A.B. Santa and H.G. Riella, A facile method for
1161 synthesis of nanostructured copper(II) oxide by co-precipitation, *J. Mater. Res.*
1162 *Technol.* 9 (2020) 994–1004.
- 1163 [37] K. Velsankar, S. Suganya, P. Muthumari, S. Mohandoss and S. Sudhahar,
1164 Ecofriendly green synthesis, characterization and biomedical applications of
1165 CuO nanoparticles synthesized using leaf extract of *Capsicum frutescens*, *J.*
1166 *Environ. Chem. Eng.* 9 (2021) 106299.
- 1167 [38] A. Waris, M. Din, A. Ali, M. Ali, S. Afridi, A. Baset and A. U. Khan, A
1168 comprehensive review of green synthesis of copper oxide nanoparticles and their
1169 diverse biomedical applications, *Inorg. Chem. Commun.* 123 (2021) 1387–7003.

- 1170 [39] D. Rehana, D. Mahendiran, R. S. Kumar and A. K. Rahiman, Evaluation of
1171 antioxidant and anticancer activity of copper oxide nanoparticles synthesized
1172 using medicinally important plant extracts, *Biomed. Pharmacother.* 89 (2017)
1173 1067–1077.
- 1174 [40] S.S. Salem and A. Fouda, Green synthesis of metallic nanoparticles and
1175 their prospective biotechnological applications: an overview, *Biol. Trace Elem.*
1176 *Res.* 199 (2021) 344–370.
- 1177 [41] M. Naseer, U. Aslam, B. Khalid and B. Chen, Green route to synthesize
1178 Zinc Oxide Nanoparticles using leaf extracts of *Cassia fistula* and *Melia azadarach*
1179 and their antibacterial potential, *Sci. Rep.* 10 (2020) 1–10.
- 1180 [42] C. Dipankar and S. Murugan, The green synthesis, characterization and
1181 evaluation of the biological activities of silver nanoparticles synthesized from
1182 *Iresine herbstii* leaf aqueous extracts, *Colloids Surf., B.* 98 (2012) 112–119.
- 1183 [43] R. Javed, M. Ahmed, I. ul Haq, S. Nisa and M. Zia, PVP and PEG doped
1184 CuO nanoparticles are more biologically active: Antibacterial, antioxidant,
1185 antidiabetic and cytotoxic perspective, *Mater. Sci. Eng., C.* 79 (2017) 108–115.
- 1186 [44] M.N. Karim, M. Singh, P. Weerathunge, P. Bian, R. Zheng, C. Dekiwadia,
1187 T. Ahmed, S. Walia, E. Della Gaspera and S. Singh, Visible-light-triggered
1188 reactive-oxygen-species mediated antibacterial activity of peroxidase-mimic CuO
1189 nanorods, *ACS Appl. Nano Mater.* 1 (2018) 1694–1704.
- 1190 [45] S. Kabir, R. Cueto, S. Balamurugan, L.D. Romeo, J.T. Kuttruff, B.D. Marx,
1191 I.I. Negulescu, Removal of acid dyes from textile wastewaters using fish scales
1192 by absorption process, *Clean Technol.* 1 (1) (2019) 311–324.
- 1193 [46] T.U. Rashid, S.F. Kabir, M.C. Biswas, M.R. Bhuiyan, Sustainable
1194 wastewater treatment via dye–surfactant interaction: a critical review, *Ind. Eng.*
1195 *Chem. Res.* 59 (21) (2020) 9719–9745.
- 1196 [47] F. Qu, A. Cao, Y. Yang, S. Mahmud, P. Su, J. Yang, Z. He, Q. Lai, L. Zhu,
1197 Z. Tu, Q. Wang, Z. Xiong, S. Zhao, Hierarchically superhydrophilic
1198 poly(vinylidene fluoride) membrane with self-cleaning fabricated by surface
1199 mineralization for stable separation of oily wastewater, *J. Membr. Sci.* 640 (2021)
1200 119864.
- 1201 [48] F. Ghanbari, M. Moradi, *Electrooxidation Processes for Dye Degradation*
1202 *and Colored Wastewater Treatment.* CRC Press LLC, London (2016).
- 1203 [49] J. Dotto, M.R. Fagundes-Klen, M.T. Veit, S.M. Palacio, R. Bergamasco,
1204 Performance of different coagulants in the coagulation/flocculation process of
1205 textile wastewater, *J. Cleaner Prod.* 208 (2019) 656–665.

- 1206 [50] P.S. Kumar, A. Saravanan, Sustainable Wastewater Treatments in Textile
1207 Sector, Sustainable Fibres and Textiles. Elsevier (2017) pp. 323–346.
- 1208 [51] Y. Tian, Y. Shu, X. Zhang, S. Mahmud, J. Zhu, S. Su, Electrospun PVDF-
1209 Ag@ AgCl porous fiber membrane: stable antifoul and antibacterial surface,
1210 Surface Innov. 9 (2–3) (2020) 156–165.
- 1211 [52] X. Guo, S. Mahmud, X. Zhang, N. Yu, K.F. Hasan, One-pot green synthesis
1212 of Ag@ AgCl nanoparticles with excellent photocatalytic performance, Surface
1213 Innov. 9 (5) (2021) 277–284.
- 1214 [53] A. Akbari, M. Amini, A. Tarassoli, B. Eftekhari-Sis, N. Ghasemian, E.
1215 Jabbari, Transition metal oxide nanoparticles as efficient catalysts in oxidation
1216 reactions, Nano-Struct. Nano-Objects 14 (2018) 19–48.
- 1217 [54] M. Nasrollahzadeh, M. Sajjadi, S. Iravani, R.S. Varma, Carbon-based
1218 sustainable nanomaterials for water treatment: State-of-art and future
1219 perspectives, Chemosp. 263 (2021a) 128005.
- 1220 [55] M. Nasrollahzadeh, M. Sajjadi, S. Iravani, R.S. Varma, Green-synthesized
1221 nanocatalysts and nanomaterials for water treatment: Current challenges and
1222 future perspectives, J. Hard Mater. 401 (2021b) 123401.
- 1223 [56] M. Sorbiun, E. S. Mehr, A. Ramazani and S. T. Fardood, Green synthesis of
1224 zinc oxide and copper oxide nanoparticles using aqueous extract of oak fruit hull
1225 (jaft) and comparing their photocatalytic degradation of basic violet 3, Int. J.
1226 Environ. Res. 12 (2018) 29–37.
- 1227 [57] E.S. Mehr, M. Sorbiun, A. Ramazani and S. T. Fardood, Plant-mediated
1228 synthesis of zinc oxide and copper oxide nanoparticles by using *Ferula goangulata*
1229 (schlecht) boiss extract and comparison of their photocatalytic degradation of
1230 Rhodamine B (RhB) under visible light irradiation, J. Mater. Sci.: Mater. Electron.
1231 29 (2018) 1333–1340.
- 1232 [58] A. Muthuvel, M. Jothibas and C. Manoharan, Synthesis of copper oxide
1233 nanoparticles by chemical and biogenic methods: photocatalytic degradation and
1234 in vitro antioxidant activity, Nanotechnol. Environ. Eng. 5 (2020) 1–19.
- 1235 [59] G. Bibi, N. Ullah, A. Mannan and B. Mirza, Antitumor, cytotoxic and
1236 antioxidant potential of *Aster thomsonii* extracts, Afr. J. Pharm. Pharmacol. 5
1237 (2011) 252–258.
- 1238 [60] M.A. Sheliya, R. Begum, K.K. Pillai, V. Aeri, S.R. Mir, A. Ali, M. Sharma,
1239 In vitro α -glucosidase and α -amylase inhibition by aqueous, hydroalcoholic, and
1240 alcoholic extract of *Euphorbia hirta* L., Drug Dev. Ther. 7 (2016) 26.

- 1241 [61] B. Saleem, M. Islam, H. Saeed, F. Imtiaz, M. Asghar, Z. Saleem, A.
1242 Mehmood, S. Naheed, Investigations of *Acacia modesta* Wall. leaves for *in vitro*
1243 antidiabetic, proliferative and cytotoxic effects, *Braz. J. Pharm. Sci.* 54 (2018) 2.
- 1244 [62] M. Biglar, K. Soltani, F. Nabati, R. Bazl, F. Mojab and M. Amanlou, A
1245 preliminary investigation of the jack-bean urease inhibition by randomly selected
1246 traditionally used herbal medicine, *Iran. J. Pharm. Res.* 11 (2012) 831.
- 1247 [63] G. J. McDougall, N. N. Kulkarni and D. Stewart, Berry polyphenols inhibit
1248 pancreatic lipase activity *in vitro*, *Food Chem.* 115 (2009) 193–199.
- 1249 [64] H. Fatima, K. Khan, M. Zia, T. Ur-Rehman, B. Mirza and I.-u. Haq,
1250 Extraction optimization of medicinally important metabolites from *Datura*
1251 *innoxia* Mill.: an *in vitro* biological and phytochemical investigation, *BMC*
1252 *Complementary Altern. Med.* 15 (2015) 1–18.
- 1253 [65] H. Zafar, A. Ali, J. S. Ali, I. U. Haq and M. Zia, Effect of ZnO nanoparticles
1254 on *Brassica nigra* seedlings and stem explants: growth dynamics and
1255 antioxidative response, *Front. Plant Sci.* 7 (2016) 535.
- 1256 [66] M. Shah, M.A. Ullah, S. Drouet, M. Younas, D. Tungmunnithum, N.
1257 Giglioli-Guivar ch, C. Hano and B.H. Abbasi, Interactive effects of light and
1258 melatonin on biosynthesis of silymarin and anti-inflammatory potential in callus
1259 cultures of *Silybum marianum* (L.) Gaertn, *Molecules* 24 (2019) 1207.
- 1260 [67] M. Nazir, D. Tungmunnithum, S. Bose, S. Drouet, L. Garros, N. Giglioli-
1261 Guivar ch, B. H. Abbasi and C. Hano, Differential production of phenylpropanoid
1262 metabolites in callus cultures of *Ocimum basilicum* L. with distinct *in vitro*
1263 antioxidant activities and *in vivo* protective effects against UV stress, *J. Agric.*
1264 *Food Chem.* 67 (2019) 1847–1859.
- 1265 [68] B. Shanmuganathan, K. Pandima Devi, Evaluation of the nutritional
1266 profile and antioxidant and anti-cholinesterase activities of *Padina gymnospora*
1267 (Phaeophyceae), *Eur J Phycol.* 51 (2016) 482–490. [https://doi.org/10.1080/09670](https://doi.org/10.1080/09670262.2016.1218938)
1268 [262.2016.1218938](https://doi.org/10.1080/09670262.2016.1218938).
- 1269 [69] R.J. Ruch, S.J. Cheng, J.E. Klaunig, Prevention of cytotoxicity and
1270 inhibition of intercellular communication by antioxidant catechins isolated from
1271 Chinese green tea, *Carcinogen* 10 (1989) 1003-1008.
- 1272 [70] L. Lagrimini, Plant peroxidases: under- and over-expression in transgenic
1273 plants and physiological consequences, *Plant Peroxidases* 1980 (1990) 59–69.
- 1274 [71] V. De Matteis, M. Cascione, C.C. Toma, S. Leporatti, Silver nanoparticles:
1275 synthetic routes, *in vitro* toxicity and theranostic applications for cancer disease,
1276 *Nanomaterials (Basel)* 8 (2018) 319. doi:10.3390/nano8050319.

- 1277 [72] C.N. Baker, S.A. Stocker, D.H. Culver, C. Thornsberry, Comparison of the
1278 E Test to agar dilution, broth microdilution, and agar diffusion susceptibility
1279 testing techniques by using a special challenge set of bacteria, *J. Clin. Microbiol.*
1280 29 (1991) 533–538.
- 1281 [73] J. Hausdorfer, E. Sompek, F. Allerberger, M. Dierich, S. Rüscher-Gerdes, E-
1282 test for susceptibility testing of *Mycobacterium tuberculosis*, *Int. J. Tuberc. Lung*
1283 *Dis.* 2 (1998) 751–755.
- 1284 [74] S. Magaldi, S. Mata-Essayag, C.H. de Capriles, C. Pérez, M. Colella, C.
1285 Olaizola, Y. Ontiveros, Well diffusion for antifungal susceptibility testing, *Int. J.*
1286 *Infect. Dis.* 8 (2004) 39–45.
- 1287 [75] C. Valgas, S.M.d. Souza, E.F. Smânia, A. Jr. Smânia, Screening methods to
1288 determine antibacterial activity of natural products, *Braz. J. Microbiol.* 38 (2007)
1289 369–380.
- 1290 [76] F. Duman, I. Ocsoy, F.O. Kup, Chamomile flower extract-directed CuO
1291 nanoparticle formation for its antioxidant and DNA cleavage properties, *Mater.*
1292 *Sci. Eng. C* 60 (2016) 333–338.
- 1293 [77] S.-H. Kim, H.-S. Lee, D.-S. Ryu, S.-J. Choi, D.-S. Lee, Antibacterial activity
1294 of silver-nanoparticles against *Staphylococcus aureus* and *Escherichia coli*,
1295 *Microbiol. Biotechnol. Lett.* 39 (2011) 77–85.
- 1296 [78] A. Álvarez-Ordóñez, A. Carvajal, H. Arguello, F. Martínez-Lobo, G.
1297 Naharro, P. Rubio, Antibacterial activity and mode of action of a commercial
1298 citrus fruit extract, *J. Appl. Microbiol.* 115 (2013) 50–60.
- 1299 [79] S. Lee, K. Na, Oleic acid conjugated polymeric photosensitizer for
1300 metastatic cancer targeting in photodynamic therapy, *Biomater. Res.* 24 (2020) 1–
1301 8.
- 1302 [80] X. Deng, M. Cao, J. Zhang, K. Hu, Z. Yin, Z. Zhou, X. Xiao, Y. Yang, W.
1303 Sheng, Y. Wu, *et al.*, Hyaluronic acid-chitosan nanoparticles for co-delivery of
1304 MiR-34a and doxorubicin in therapy against triple negative breast cancer,
1305 *Biomaterials* 35 (2014) 4333–4344.
- 1306 [81] S. Blanco, S. Peralta, M.E. Morales, E. Martínez-Lara, J.R. Pedrajas, H.
1307 Castán, M.Á. Peinado, M.A. Ruiz, Hyaluronate nanoparticles as a delivery
1308 system to carry neuroglobin to the brain after stroke, *Pharmaceutics* 12 (1) (2020)
1309 40.
- 1310 [82] C. Saraiva, C. Praca, R. Ferreira, T. Santos, L. Ferreira, L. Bernardino,
1311 Nanoparticle-mediated brain drug delivery: Overcoming blood-brain barrier to
1312 treat neurodegenerative diseases, *J. Control. Release.* 235 (2016) 34–47.

- 1313 [83] K. Ganesan, V.K. Jothi, A. Natarajan, A. Rajaram, S. Ravichandran, S.
1314 Ramalingam, Green synthesis of Copper oxide nanoparticles decorated with
1315 graphene oxide for anticancer activity and catalytic applications, *Arabian J.*
1316 *Chem.* 13 (2020) 6802–6814.
- 1317 [84] N.M. Zain, A.G.F. Stapley, G. Shama, Green synthesis of silver and copper
1318 nanoparticles using ascorbic acid and chitosan for antimicrobial applications,
1319 *Carbohydr. Polym.* 112 (2014) 195–202, doi:10.1016/j.carbpol.2014.05.081.
- 1320 [85] S. Chaudhary, D. Rohilla, A. Umar, N. Kaur, A. Shanavas, Synthesis and
1321 characterizations of luminescent copper oxide nanoparticles: toxicological
1322 profiling and sensing applications, *Ceram. Int.* 45 (2019) 15025–15035.
- 1323 [86] A. Shafiq, A.A. Aziz, B. Mehrdel, Nanoparticle optical properties: Size
1324 dependence of a single gold spherical nanoparticle, *Journal of Physics:*
1325 *Conference Series.* IOP Publishing (2018) 012040.
- 1326 [87] S.K. Das, B.K. Chandra, R.A. Molla, M. Sengupta, S.M. Islam, A. Majee, A.
1327 Bhaumik, CuO grafted triazine functionalized covalent organic framework as an
1328 efficient catalyst for CC homo coupling reaction, *Mol. Catal.* 480 (2020) 110650.
- 1329 [88] M. Guo, W. Li, F. Yang, H. Liu, Controllable biosynthesis of gold
1330 nanoparticles from a *Eucommia ulmoides* bark aqueous extract, *Spectrochim. Acta*
1331 *Part A: Mol. Biomol. Spectr.* 142 (2015) 73–79.
- 1332 [89] K. Kartini, A. Alviani, D. Anjarwati, A.F. Fanany, J. Sukweenadhi, and C.
1333 Avanti, Process optimization for green synthesis of silver nanoparticles using
1334 Indonesian medicinal plant extracts, *Processes* 8 (8) (2020) 998.
1335 doi:10.3390/pr8080998.
- 1336 [90] P.K. Dikshit, J. Kumar, A.K. Das, S. Sadhu, S. Sharma, S. Singh, P.K. Gupta
1337 and B.S. Kim, Green synthesis of metallic nanoparticles: Applications and
1338 Limitations, *Catalysts* 11 (8) (2021) 902; <https://doi.org/10.3390/catal11080902>.
- 1339 [91] M.M. Said, M. Rehan, S.M. El-Sheikh, M.K. Zahran, M.S. Abdel-Aziz, M.
1340 Bechelany, A. Barhoum, Multifunctional hydroxyapatite/silver
1341 nanoparticles/cotton gauze for antimicrobial and biomedical applications,
1342 *Nanomaterials* 11 (2021) 429.
- 1343 [92] Q. Song, Y. Wang, L. Huang, M. Shen, Y. Yu, Q. Yu, Y. Chen, J. Xie,
1344 Review of the relationships among polysaccharides, gut microbiota, and human
1345 health, *Food Res. Int.* 140 (2021) 109858.
- 1346 [93] M. Fernandes, A.P. Souto, F. Dourado, M. Gama, Application of bacterial
1347 cellulose in the Textile and Shoe Industry: Development of biocomposites,
1348 *Polysaccharides* 2 (2021) 34.

- 1349 [94] R. Mongkhlorattanasit, C. Klaichoi, N. Rungruangkitkrai, Printing silk
1350 fabric with acid dye using a new thickening agent, *J. Nat. Fibers* (2021) in press.
- 1351 [95] H. Chen, Y. Jia, Q. Guo, Polysaccharides and polysaccharide complexes as
1352 potential sources of antidiabetic compounds: A review. In *Bioactive Natural*
1353 *Products*; Atta-ur-Rahman, Ed.; Studies in Natural Products Chemistry; Elsevier:
1354 Amsterdam, The Netherlands (2020) 199–220.
- 1355 [96] C. Wang, X. Gao, Z. Chen, Y. Chen, H. Chen, Preparation, characterization
1356 and application of polysaccharide-based metallic nanoparticles: A review,
1357 *Polymers* 9 (2017) 689.
- 1358 [97] M. Fernandes, J. Padrão, A.I. Ribeiro, R.D.V. Fernandes, L. Melro, T.
1359 Nicolau, B. Mehravani, C. Alves, R. Rodrigues and A. Zille, Polysaccharides and
1360 metal nanoparticles for functional textiles: A review, *Nanomaterials* 12 (6) (2022)
1361 1006; <https://doi.org/10.3390/nano12061006>.
- 1362 [98] D.O.B. Apriandanu and Y. Yulizar, *Tinospora crispa* leaves extract for the
1363 simple preparation method of CuO nanoparticles and its characterization, *Nano-*
1364 *Struct. Nano- Objects*, 20 (2019) 100401.
- 1365 [99] Y. Yulizar, I. Latifah, R. Bakri and D. Apriandanu, Plants extract mediated
1366 synthesis of copper (II) oxide nanoparticles using *Oldenlandia corymbosa* L. leaf,
1367 *AIP Conf. Proc.* 2023 (2018) 020097.
- 1368 [100] J. Iqbal, A. Andleeb, H. Ashraf, B. Meer, A. Mehmood, H. Jan, G. Zaman,
1369 M. Nadeem, S. Drouet, H. Fazal, N.G.-Guivarch, C. Hano and B.H. Abbasi,
1370 Potential antimicrobial, antidiabetic, catalytic, antioxidant and ROS/RNS
1371 inhibitory activities of *Silybum marianum* mediated biosynthesized copper oxide
1372 nanoparticles, *RSC Adv.* 12 (2022) 14069–14083.
- 1373 [101] J. Wongpreecha, D. Polpanich, T. Suteewong, C. Kaewsaneha, P.
1374 Tangboriboonrat, One-pot, large-scale green synthesis of silver nanoparticles-
1375 chitosan with enhanced antibacterial activity and low cytotoxicity, *Carbohydr.*
1376 *Polymers* 199 (2018) 641–648.
- 1377 [102] A. Nair, C. Jayakumari, P. Jabbar, R. Jayakumar, N. Raizada, A. Gopi, G. S.
1378 George and T. Seenaa, Prevalence and associations of hypothyroidism in Indian
1379 patients with type 2 diabetes mellitus, *J. Thyroid Res.* 2018 (2018) 7.
- 1380 [103] S. Ghosh, P. More, R. Nitnavare, S. Jagtap, R. Chippalkatti, A. Derle, R.
1381 Kitture, A. Asok, S. Kale and S. Singh, Antidiabetic and antioxidant properties of
1382 copper nanoparticles synthesized by medicinal plant *Dioscorea bulbifera*, *J.*
1383 *Nanomed. Nanotechnol.* S6 (2015) 1–9.
- 1384 [104] U. Shwetha, M. Latha, C. R. Kumar, M. Kiran, H. Onkarappa and V. S.
1385 Betageri, Potential antidiabetic and anticancer activity of copper oxide

- 1386 nanoparticles synthesised using *Areca catechu* leaf extract, *Adv. Nat. Sci.:*
1387 *Nanosci. Nanotechnol.* 12 (2021) 025008.
- 1388 [105] W.D. Seo, J.H. Kim, J.E. Kang, H.W. Ryu, M.J. Curtis-Long, H.S. Lee, M.S.
1389 Yang, K.H. Park, Sulfonamide Chalcone as a new class of alpha-glucosidase
1390 inhibitors, *Bioorg. Med. Chem. Lett.* 15 (24) (2005) 5514–5516.
- 1391 [106] J.P. Saludes, S.C. Lievens, T.F. Molinski, Occurrence of the alpha-
1392 glucosidase inhibitor 1,4-Dideoxy-1,4-imino-D-arabinitoland related
1393 iminopentitols in marine sponges, *J. Natural Products.* 70 (3) (2007) 436–438.
- 1394 [107] N.U. Islam, R. Amin, M. Shahid, M. Amin, S. Zaib and J. Iqbal, A multi-
1395 target therapeutic potential of *Prunus domestica* gum stabilized nanoparticles
1396 exhibited prospective anticancer, antibacterial, urease-inhibition, anti-
1397 inflammatory and analgesic properties, *BMC Complementary Altern. Med.* 17
1398 (2017) 1–17.
- 1399 [108] Sachan S. and A. Singh, Lipase enzyme and its diverse role in food
1400 processing industry, *Everyman's Sci.* 4 (2015) 214–218.
- 1401 [109] M. I. Choudhary, M. Ali, A.-T. Wahab, A. Khan, S. Rasheed, S. L. Shyaula
1402 and A.-U. Rahman, New antiglycation and enzyme inhibitors from *Parmotrema*
1403 *cooperi*, *Sci. China: Chem.* 54 (2011) 1926–1931.
- 1404 [110] W.I. Abdel-Fattah, G.W. Ali, Anti-cancer activities of silver nanoparticles,
1405 *J. Appl. Biotechnol. Bioeng.* 5 (2018) 00116.
- 1406 [111] P. Rameshthangam, J.P. Chitra, Synergistic anticancer effect of green
1407 synthesized nickel nanoparticles and quercetin extracted from *Ocimum sanctum*
1408 leaf extract, *J. Materials Sci & Tech.* 34 (2018) 508–522.
- 1409 [112] F. Ibraheem, M.H. Aziz, M. Fatima, F. Shaheen, S.M. Ali, Q. Huang, In
1410 vitro Cytotoxicity, MMP and ROS activity of green synthesized nickel oxide
1411 nanoparticles using extract of *Terminalia chebula* against MCF-7 cells, *Materials*
1412 *Lett.* 234 (2019) 129–133.
- 1413 [113] R. Sankar, R. Maheswari, S. Karthik, *et al.*, Anticancer activity of *Ficus*
1414 *religiosa* engineered copper oxide nanoparticles, *Mat Sci Eng C.* 44 (2014) 234–239.
- 1415 [114] M. Baghayeri, B. Mahdavi, Z. Hosseinpor-Mohsen Abadi, S. Farhadi,
1416 Green synthesis of silver nanoparticles using water extract of *Salvia leriifolia*:
1417 Antibacterial studies and applications as catalysts in the electrochemical
1418 detection of nitrite, *Appl. Organomet. Chem.* 32 (2018) e4057.
- 1419 [115] K. Sridhar, A.L. Charles, In vitro antioxidant activity of Kyoho grape
1420 extracts in DPPH and ABTS assays: Estimation methods for EC50 using
1421 advanced statistical programs, *Food Chem.* 275 (2019) 41–49. doi:
1422 10.1016/j.foodchem.2018.09.040.

- 1423 [116] R. Subramanian, P. Subbramaniyan, V. Raj, Antioxidant activity of the
1424 stem bark of *Shorea roxburghii* and its silver reducing power, Springer Plus 2 (1)
1425 (2013) 28.
- 1426 [117] P. Khandel, S.K. Shahi, D.K. Soni, R.K. Yadaw and L. Kanwar, *Alpinia*
1427 *calcarata*: potential source for the fabrication of bioactive silver nanoparticles,
1428 Nano Convergence 5 (2018) 37. <https://doi.org/10.1186/s40580-018-0167-9>.
- 1429 [118] M. Shah, S. Nawaz, H. Jan, N. Uddin, A. Ali, S. Anjum, N. Giglioli-
1430 Guivarc'h, C. Hano and B. H. Abbasi, Synthesis of bio-mediated silver
1431 nanoparticles from *Silybum marianum* and their biological and clinical activities,
1432 Mater. Sci. Eng., C. 112 (2020) 110889.
- 1433 [119] S. Sangami, B. Manu, Synthesis of green iron nanoparticles using laterite
1434 and their application as a Fenton-like catalyst for the degradation of herbicide
1435 ametryn in water, Environ Technol Innov. 8 (2017) 150–163.
- 1436 [120] L. Katata-Seru, T. Moremedi, O.S. Aremu, I. Bahadur, Green synthesis of
1437 iron nanoparticles using *Moringa oleifera* extracts and their applications: Removal
1438 of nitrate from water and antibacterial activity against *Escherichia coli*, J Mol Liq.
1439 256 (2018) 296–304.
- 1440 [121] N. Beheshtkhoo, M.A.J. Kouhbanani, A. Savardashtaki, A.M. Amani, S.
1441 Taghizadeh, Green synthesis of iron oxide nanoparticles by aqueous leaf extract
1442 of *Daphne mezereum* as a novel dye removing material, Appl. Phys A. 124 (2018)
1443 363–369.
- 1444 [122] I.A. Radini, N. Hasan, M.A. Malik, Z. Khan, Biosynthesis of iron
1445 nanoparticles using *Trigonella foenum-graecum* seed extract for photocatalytic
1446 methyl orange dye degradation and antibacterial applications, J Photochem
1447 Photobiol B. 183 (2018) 154–163.
- 1448 [123] C.A. Sousa, H.M. Soares and E.V. Soares, Nickel oxide (NiO) nanoparticles
1449 induce loss of cell viability in yeast mediated by oxidative stress, Chem. Res.
1450 Toxicol. 31 (2018) 658–665.
- 1451 [124] W. Jansen, J. Van Der Bruggen, J. Verhoef, A. Fluit, Bacterial resistance: a
1452 sensitive issue: complexity of the challenge and containment strategy in Europe,
1453 Drug Resist. Updat. 9 (2006) 123–133.
- 1454 [125] M. Behravan, A.H. Panahi, A. Naghizadeh, M. Ziaee, R. Mahdavi, A.
1455 Mirzapour, Facile green synthesis of silver nanoparticles using *Berberis vulgaris*
1456 leaf and root aqueous extract and its antibacterial activity, Internat J. Biological
1457 Macromol. 124 (2019) 148–154.

- 1458 [126] B.S. Atiyeh, M. Costagliola, S.N. Hayek, S.A. Dibo, Effect of silver on burn
1459 wound infection control and healing: review of the literature, *Burns* 33 (2007)
1460 139–148.
- 1461 [127] M.M. Mohamed, S.A. Fouad, H.A. Elshoky, G.M. Mohammed, T.A.
1462 Salaheldin, Antibacterial effect of gold nanoparticles against *Corynebacterium*
1463 *pseudotuberculosis*, *Int. J. Vet. Sci. Med.* 5 (1) (2017) 23–29.
- 1464 [128] P. Senthilkumar, L. Surendran, B. Sudhagar, D. S. Ranjith Santhosh
1465 Kumar, Facile green synthesis of gold nanoparticles from marine algae *Gelidiella*
1466 *acerosa* and evaluation of its biological potential, *SN Applied Sci.* 1 (2019) 284.
1467 <https://doi.org/10.1007/s42452-019-0284-z>.
- 1468 [129] I. Sondi and B. Salopek-Sondi, Silver nanoparticles as antimicrobial agent:
1469 a case study on *E. coli* as a model for Gram-negative bacteria, *J. Colloid Interface*
1470 *Sci.* 275 (2004) 177–182.
- 1471 [130] G. Ren, D. Hu, E. W. Cheng, M.A. Vargas-Reus, P. Reip and R.P. Allaker,
1472 Characterisation of copper oxide nanoparticles for antimicrobial applications, *Int.*
1473 *J. Antimicrob. Agents.* 33 (2009) 587–590.
- 1474 [131] S. Jadhav, S. Gaikwad, M. Nimse and A. Rajbhoj, Copper oxide
1475 nanoparticles: synthesis, characterization and their antibacterial activity, *J.*
1476 *Cluster Sci.* 22 (2011) 121–129.
- 1477 [132] Y.-N. Chang, M. Zhang, L. Xia, J. Zhang and G. Xing, The toxic effects and
1478 mechanisms of CuO and ZnO nanoparticles, *Materials* 5 (2012) 2850–2871.
- 1479 [133] L. Karygianni, Z. Ren, H. Koo, T. Thurnheer, Biofilm Matrixome:
1480 Extracellular components in structured microbial communities, *Trends*
1481 *Microbiol.* 28 (8) (2020) 668–681.
- 1482 [134] A.S. Joshi, P. Singh, I. Mijakovic, Interactions of gold and silver
1483 nanoparticles with bacterial biofilms: Molecular interactions behind inhibition
1484 and resistance, *Int. J. Mol. Sci.* 21 (20) (2020) 7658.
- 1485 [135] S. Oliver, H. Wagh, Y. Liang, S. Yang and C. Boyer, Enhancing the
1486 antimicrobial and antibiofilm effectiveness of silver nanoparticles prepared by
1487 green synthesis, *J. Mater. Chem. B.* 6 (2018) 4124–4138.
- 1488 [136] M.A. El-ghamry, K.M. Nassir, F.M. Elzawawi, A.A. Abdel Aziz, S.M. Abu-
1489 El-Wafa, Novel nanoparticle-size metal complexes derived from acyclovir.
1490 Spectroscopic characterization, thermal analysis, antitumor screening, and DNA
1491 cleavage, as well as 3D modeling, docking, and electrical conductivity studies, *J.*
1492 *Molecular Struct.* 1235 (2021) 130235.
- 1493 [137] F. Gulbagca, A. Aygün, M. Gülcan, S. Ozdemir, S. Gonca, F. Şen, Green
1494 synthesis of palladium nanoparticles: Preparation, characterization, and

- 1495 investigation of antioxidant, antimicrobial, anticancer, and DNA cleavage
1496 activities, *Appl Organomet Chem.* (2021) e6272. <https://doi.org/10.1002/aoc.6272>.
- 1497 [138] M.Y. Begum, Y. Alhamhoom and A. Roy, Study of antimicrobial and DNA
1498 cleavage property of biocompatible silver nanoparticles prepared by using *Ficus*
1499 *carica* L., *Materials Res Innovat.* (2020) DOI: 10.1080/14328917.2020.1753335.
- 1500 [139] S. Ravichandran, V. Paluri, G. Kumar, K. Loganathan, B.R. Kokati
1501 Venkata, A novel approach for the biosynthesis of silver oxide nanoparticles
1502 using aqueous leaf extract of *Callistemon lanceolatus* (Myrtaceae) and their
1503 therapeutic potential, *J. Exp. Nanosci.* 11 (2016) 445–458.
- 1504 [140] E. Dilshad, M. Bibi, N.A. Sheikh, K.F. Tamrin, Q. Mansoor, Q. Maqbool
1505 and M. Nawaz, Synthesis of functional silver nanoparticles and microparticles
1506 with modifiers and evaluation of their antimicrobial, anticancer, and antioxidant
1507 activity, *J. Funct. Biomater.* 11 (2020) 76; doi:10.3390/jfb11040076.
- 1508 [141] Z. He, S. Mahmud, Y. Yang, L. Zhu, Y. Zhao, Q. Zeng, Z. Xiong, S. Zhao,
1509 Polyvinylidene fluoride membrane functionalized with zero valent iron for
1510 highly efficient degradation of organic contaminants, *Separ. Purif. Technol.* 250
1511 (2020a) 117266.
- 1512 [142] Z. He, S. Mahmud, S. Zhao, Y. Yang, L. Zhu, Y. Zhao, Q. Zeng, Z. Xiong,
1513 C. Hu, Hierarchically active poly(vinylidene fluoride) membrane fabricated by in
1514 situ generated zero-valent iron for fouling reduction, *ACS Appl. Mater. Interf.* 12
1515 (9) (2020b) 10993–11004.
- 1516 [143] Y. Zhong, S. Mahmud, Z. He, Y. Yang, Z. Zhang, F. Guo, Z. Chen, Z.
1517 Xiong, Y. Zhao, Graphene oxide modified membrane for highly efficient
1518 wastewater treatment by dynamic combination of nanofiltration and catalysis, *J.*
1519 *Hard Mater.* 397 (2020) 122774.
- 1520 [144] H. Wang, G. Zhang, R. Mia, W. Wang, L. Xie, S. Lü, S. Mahmud, H. Liu,
1521 Bioreduction (Ag^+ to Ag^0) and stabilization of silver nanocatalyst using
1522 hyaluronate biopolymer for azo-contaminated wastewater treatment, *J. Alloys*
1523 *Comp.* 894 (2022) 162502.
- 1524 [145] S. Pandey, J.Y. Do, J. Kim, M. Kang, Fast and highly efficient catalytic
1525 degradation of dyes using κ -carrageenan stabilized silver nanoparticles
1526 nanocatalyst, *Carbohydr. Polym.* 230 (2020) 115597.
- 1527 [146] J. Li, C.-Y. Liu, Y. Liu, Au/graphene hydrogel: synthesis, characterization
1528 and its use for catalytic reduction of 4-nitrophenol, *J. Mater. Chem.* 22 (2012)
1529 8426–8430.